بسم الله الرحمن الرحيم

Sudan University of Sciences and Technology

College of Graduate Studies

Estimation of Patients Dose during Paranasal Sinuses Examinations using Computed Tomography

تقدير الجرعة الإشعاعية للمرضي اثناء اختبارات الجيوب الأنفية بإستخدام التصوير المقطعي

A thesis Submitted for the Partial Fulfillment of the M.Sc Degree in

Diagnostic Radiology

By:

Fatima Saad Albashir Alsiddig

Supervisor:

Dr. Asma Ibrahim Ahmed Alamin

2018

الآيـــــــــــــــة

قال تعالى:

(يَرْفَعِ اللَّهُ الَّذِينَ آمَنُوا مِنْكُمْ وَالَّذِينَ أُوتُوا الْعِلْمَ دَرَجَاتٍ وَاللَّهُ بِمَا تَعْمَلُونَ خَبِيرٌ)

صدق الله العظيم

(المجادلة:11)

Dedication

TO MY MOTHER

TO MY FATHER

TO MY BROTHERS

TO MY SISTERS

Acknowledgement

My full thanks to my God in everything.

My great thanks and deep gratitude to my supervisor **Dr. Asma Ibrahim Ahmed.**

I would like to thank Dr. **Mogahid Mohammed Zidan**.

My thank to the staff of Ibn ELhaithm diagnostic center.

Abstract

Using of Computed Tomography in medical diagnosis delivers high radiation dose to patients comparing with other radiological procedures. Lake of optimizing protocols could be increasing the patients radiation dose. The aim of this study to evaluate the radiation dose to patients during paranasal sinuses Computed Tomography Examinations.the data were collected from Ibn EL haitham Diagnostic Center in period from February to August 2018. A total of 50 patients were examined in CT department with Toshiba machine 4 slices. The amount of radiation dose that received from CT scan depends on dose parameters CTDIvol and DLP.

The result of the study revealed that the patients dose obtained from CT Para nasal sinuses examinations presented as mean ± standard deviation, were the patients age was 38.38 ±17.16 ,KVP 120.00±ooo, mA100.54±24.94 , exposure2388.07±3205.41,CTDIvol52.7±25.1mGy,DLP 577.1±267.43mGy.cm and ED 8.66±4.0114 mSv .

The study concluded that the selection of the most appropriate imaging modality should be performed in view of the delivered doses, required image quality and information and the clinical circumstances

المستخلص

استخدام التصوير المقطعي في التشخيص الطبي يعطي جرعة عالية من الإشعاع للمرضى مقارنة مع الفحوصات الإشعاعية الأخرى. قلة إستعمال البروتوكولات المثالية يمكن أن تزيد من جرعة إشعاع المرضى. الهدف من هذه الدراسة هو تقييم الجرعة الإشعاعية للمرضى خلال الاختبارات التصويرية المقطعية للجيوب الأنفية . تم جمع البيانات من مركز ابن الهيثم التشخيصي في الفترة من فبراير إلى أغسطس عام 2018. تم فحص مجموعه 50 مريضا في قسم التصوير المقطعي بجهاز توشيبا الذي يحتوي غلى 4 شرائح. تعتمد كمية الجرعة الإشعاعية المأخوذة من مسح التصوير المقطعي بالكمبيوتر على معلمات الجرعة وحدة قياس حجم التصوير المقطعي ومنتج طول الجرعة.

وكشفت نتائج الدراسة أن جرعة المرضى التي تم الحصول عليها من اختبارات الجيوب الأنفية المقطعية المقدمة كالمتوسط ±الانحراف المعياري ، كان عمر المرضى 38.38± 17.16، KVP ooo ± 120.00، mA100.54 ± 24.94، exposure2388.07 ± 3205.41 ، CTDIvol52.7±25.1 mGy ، طول الجرعة المنتجة267.43± 577.1 mGy.cm و Effective Dose 8.66 ± 4.0114 mSv.

وخلصت الدراسة إلى أن اختيار أنسب طريقة للتصوير يجب أن يتم في ضوء الجرعات التي يتم تسليمها وجودة الصورة المطلوبة والمعلومات والظروف السريرية.

List of Contents

List of tables

List of figures

List of abbreviations

Abbreviation	Full meaning
2-D	Two Dimensional
3-D	Three Dimensional
CT	Computed Tomography
CTDI	Computed Tomography Dose Index
CTDIvol	Computed Tomography Dose Index Volum
CTDIw	Computed Tomography Dose Index Width
DAP	Dose Area Product
DLP	Dose Length Product
ED	Effective Dose
FWHM	Full Width Half Maximum
LI	Linear Interpolation
MDCT	Multi Detector Computed Tomography
mGy	Milligray
MSAD	Multiple Scan Average Dose
MSCT	Multi Slice Computed Tomography
PNS	Para Nasal Sinuses
SCT	Spiral Computed Tomography
SFOV	Scan Field Of View
SSCT	Single Slice Computed Tomography
TLDs	Thermoluminescent Dosimeters

CHAPTER ONE

INTRODUCTION

1-1.Introduction:

Computed tomography (CT) was first introduced as a clinical tool in 1971 when Drs. Godfrey Hounsfield and James Ambrose successfully diagnosed a brain tumor in a 41year old woman. In its most basic form, a rotating X-ray beam emits ionizing radiation of a defined thickness, which is used to irradiate the patient from numerous projections. Detectors located on the other side of the patient, opposite the source of the beam, register the amount of radiation that has penetrated through the patient. By calculating these values for numerous projections, a two dimensional image of a specified thickness is generated. These images possess contrast resolution that is far superior to conventional radiography, demonstrating the ability to distinguish substances of only slightly different densities (Anne Paterson, 2001).

Once such a 2-D image is acquired, the patient is advanced through the CT gantry for a predefined distance, and then the process is repeated. This is known as "step –and-shoot" technology. Over the 20 years following its introduction, significant improvements in this technology were made. These advances were largely the result of improvements in X-ray beam emission and detector technology, matched by advances in computer technologies to facilitate the data processing of high level functions (Anne Paterson, 2001).

1-2.Problem of study:

No sufficient previous studies in such subject in Sudan and the technologists they don't follow the same protocol for the same procedures which makes differences of patient's dose.

1-3 General Objective:

The main objective of this study to estimate the patients dose during PNS CT examinations in Khartoum state.

1-4 Specific Objectives:

- Measurement of patients dose during PNS CT examinations.
- Calculate of effective dose for all patients.
- Compare the dose according to the patients age.

1-5.Overview of study:

This thesis is concerned with assessment of radiation dose at CT neck and. accordingly, it is divided into the following chapters: Chapter one is the introduction, objectives, thesis problem and outline. Chapter two contains the background: literature review, and theoretical concepts of radiation dosimetry and technique. Chapter three describes the materials and methods. Chapter four represents the results of this study. Chapter five present discussion, conclusions and Recommendations.

CHAPTER TWO

LITERATURE REVIEW

2.1 Theoretical background:

2.1.1 Principles of Computed tomography

Computed tomography (CT) was first introduced as a clinical tool in 1971 when Drs. Godfrey Hounsfield and James Ambrose successfully diagnosed a brain tumor in a 41-year-old woman. In its most basic form, a rotating X-ray beam emits ionizing radiation of a defined thickness, which is used to irradiate the patient from numerous projections. Detectors located on the other side of the patient, opposite the source of the beam, register the amount of radiation that has penetrated through the patient. By calculating these values for numerous projections, a two dimensional image of a specified thickness is generated. These images possess contrast resolution that is far superior to conventional radiography, demonstrating the ability to distinguish substances of only slightly different densities. Once such a 2-D image is acquired, the patient is advanced through the CT gantry for a predefined distance, and then the process is repeated. This is known as “step-and-shoot” technology (fig. 2-1) (G. Bongartz et al .2004).

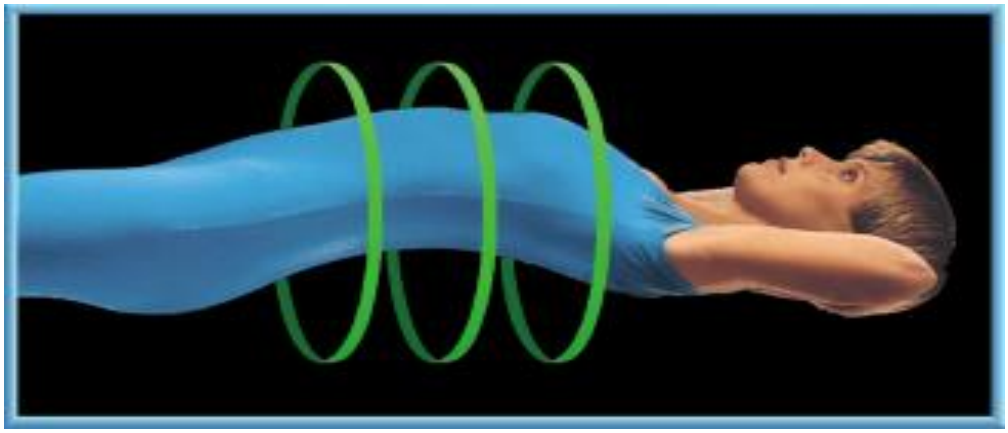

Fig (2.1) shows the step and shot technology

Over the 20 years following its introduction, significant improvements in this technology were made. These advances were largely the result of improvements

in X-ray beam emission and detector technology, matched by advances in computer technologies to facilitate the data processing of high level functions (G. Bongartz et al .2004).

2.1.2 Spiral CT imaging principles:

The old “step-and-shoot” method of CT imaging was primarily the result of the detector cables that would wind around the gantry with each beam rotation, and which needed to be “unwound” before the next slice could be acquired. The implementation of slip-ring technology eliminated this limitation, allowing for uninterrupted scanning during continuous patient advancement through the gantry, thus describing a spiral or helical pattern of data acquisition (fig. 2-2).With the introduction of spiral CT came the need to start thinking differently. It has always been necessary for radiologists to interpret images three-dimensionally. Now, however, one must think of the data acquisition itself as occurring in this way i.e. volumetrically (G. Bongartz et al .2004).

The scan parameters, which relate to this volumetric data acquisition and its processing are the subject of this chapter.

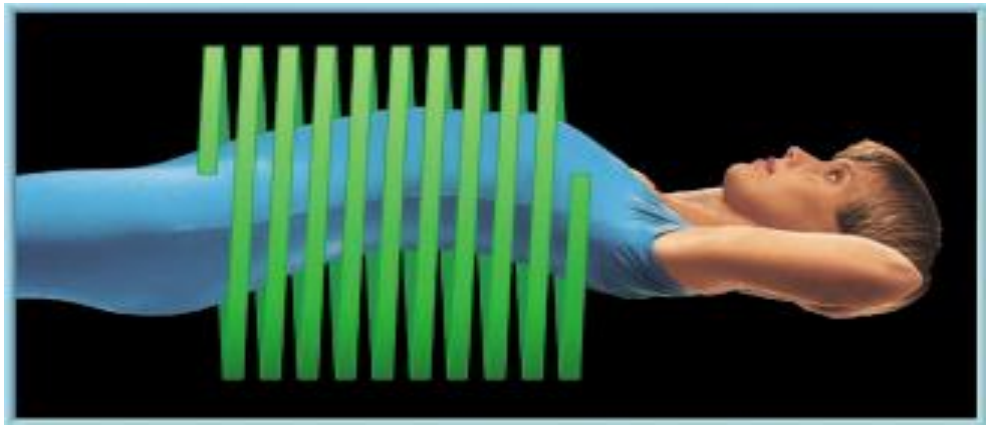

Fig (2-2) shows the Spiral CT Continuous patient motion through the gantry combined with uninterrupted beam rotation leads to the spiral pattern of data acquisition

Once a volume of data is acquired during a spiral CT (SCT) study, images can be reconstructed at any point along that volume (G. Bongartz et al .2004).

2.1.3 Multislice Volumetric Spiral CT:

Single-slice spiral CT shortened scan times by an order of magnitude compared with its predecessors. Decreasing data acquisition times from minutes to the order of second's stimulated radiologists to begin thinking physiologically as opposed to simply anatomically. It was this force that drove the industry to develop faster and more efficient scanners. The dream was to develop scanners that could be so fast as to capture volumetric data during a single breath-hold, or during a singular vascular phase-arterial, capillary, venous, or any combination. Even scan times short enough to capture a portion of a cardiac cycle were a goal. Once an efficient, extremely high powered design would be achieved, it could be employed to cover extensive volumes quickly, and with unprecedented resolution. It was these forces that lead to the development of the first multislice spiral CT unit, the Marconi MxTwin, which was introduced for clinical use in 1992. Shortly thereafter, its users became aware of the power multislice imaging possessed over the more rudimentary spiral CT scanners. The next generation of Marconi multislice scanners provides unprecedented power and speed, heralding a new era in diagnostic imaging (fig. 2-3). In single-slice spiral scanners, the X-ray tube emits a beam as it rotates around the patient. On the other side of the patient, opposite the tube, a set of detectors rotates in synchrony with the tube movement, registering the radiation that has passed through the patient. In multislice spiral CT scanners, instead of one set of detectors, there are multiple. In the first generation of multislice units (MxTwin), there are two rows of detectors, while in the second generation there are eight rows.

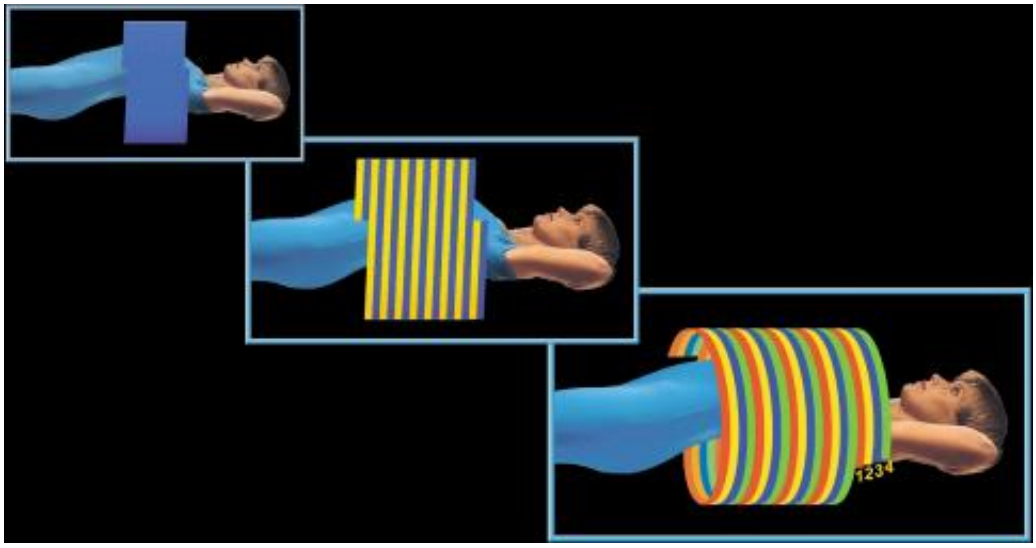

Fig (2-3) shows the Increasing from single-slice to dual-slice to quad-slice imaging increases the power, versatility, and clinical applications of the spiral technology.

These eight detectors operate in various combinations to yield up to four images per rotation, depending on the protocol chosen. All of the multislice units still employ a single radiation beam, but the key point that differentiates them from the single detector units is how that beam is utilized. For example, in a single detector unit, the tube may emit a fan beam that is approximately 5 mm thick, and the detector is collimated to register that 5mm beam, leading to the creation of a single 5mm thick image. However, in a dual detector array that same 5mm beam can now be picked up by two detectors, generating two 2.5 mm slices. In this case, the dual detectors have led to the creation of images with greater longitudinal resolution than available with the single detector units. On the other hand, if 5mm thick sections are desired, then on the MxTwin one can start with a 10mm beam that then gets split by the two detectors into two 5mm thick images. For the quadratic structure of the Mx8000, one starts with a beam that is 20mm thick. In these cases, the study can be completed in half (MxTwin) or one-quarter (Mx8000) the time as with the single-slice unit because the utilized beam is two

to four times as thick. Effective implementation of multislice imaging requires that we revisit the definition of pitch in this context. In addition, two new concepts need to be discussed since they are integral to the other image parameters employed in this technology (G. Bongartz et al .2004).

2.1.4 Detectors Design in Computed Tomography:

Modern CT systems use solid state detectors in general. Each detector element consists of a radiation-sensitive solid-state material (such as cadmium tungstate, gadolinium- oxide or gadolinium oxi-sulfide with suitable doping), which converts the absorbed X-rays into visible light. The light is then detected by a Si photodiode.

The resulting electrical current is amplified and converted into a digital signal. Key requirements for a suitable detector material are good detection efficiency, i.e., high atomic number, and very short afterglow time to enable the fast gantry rotation speeds that are essential for ECG-gated cardiac imaging. CT detectors must provide different slice widths to adjust the optimum scan speed, longitudinal resolution and image noise for each application (M. F. Reiser et al 2009).

2.1.5 Single Slice Computed Tomography verse Multi Slice Computed Tomography Detectors:

The primary difference between single-slice CT (SSCT) and MSCT hardware is in the design of the detector arrays, as illustrated in (Fig 2.4). SSCT detector arrays are one dimensional (Fig 2.4); that is, they consist of a large number (typically 750 or more) of detector elements in a single row across the irradiated slice to intercept the x-ray fan beam. In the slice thickness direction (*z*-direction), the detectors are monolithic, that is, single elements long enough (typically about 20 mm) to intercept the entire x-ray beam width, including part of the penumbra

(here, the term “x-ray beam width” always refers to the size of the x-ray beam along the *z*-axis that is, in the slice thickness direction). In MSCT, each of the individual, monolithic SSCT detector elements in the *z*-direction is divided into several smaller detector elements, forming a 2-dimensional array (Fig 2.4). Rather than a single row of detectors encompassing the fan beam, there are now multiple, parallel rows of detectors.

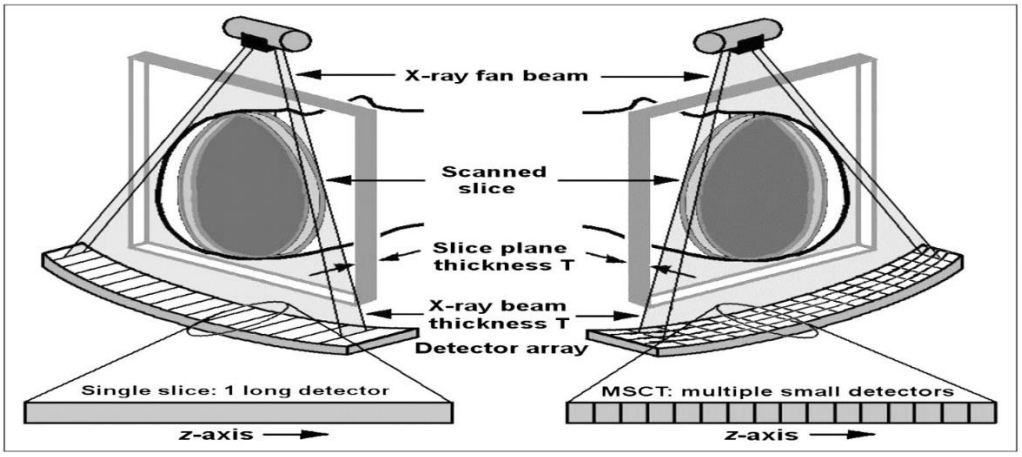

Fig (2.4) shows the (Left) SSCT arrays containing single, long elements along *z*-axis and (Right) MSCT arrays with several rows of small detector elements.

Before further discussion, a comment on nomenclature is called for: the use of the term “MSCT” is not universal. Others use the terms “multirow CT” and “multi detector row CT (MDCT)” because they are more descriptive of this technology than the term “multislice CT.” Throughout this article, however, the term “MSCT” is used.

The first scanner with more than one row of detectors and a widened *z*-axis x-ray beam was introduced by Elscint in 1992 (CT-Twin). This scanner had 2 rows of detectors, allowing data for 2 slices to be acquired simultaneously, and was developed primarily to help address the x-ray tube heating problem. The first MSCT scanner would actually be the first-generation EMI Mark 1. With 2 adjacent detectors and a widened x-ray beam, this scanner collected data for 2

slices at the same time and thereby reduced the lengthy examination time associated with the 5- to 6-min scan time. The first scanners of the "modern MSCT era" were introduced in late 1998 (Goldman 2008).

2.1.6 Multi Slice Computed tomography Data Acquisition:

A detector design used in one of the first modern MSCT scanners (Fig 2.4) consisted of 16 rows of detector elements, each 1.25 mm long in the *z*-direction, for a total *z*-axis length of 20 mm. Each of the 16 detector rows could, in principle, simultaneously collect data for 16 slices, each 1.25 mm thick; however, this approach would require handling an enormous amount of data very quickly, because a typical scanner may acquire 1,000 views per rotation. If there are 800 detectors per row and 16 rows, then almost 13 million measurements must be made during a single rotation with a duration of as short as 0.5 s.

Because of the initial limitations in acquiring and handling such large amounts of data, the first versions of modern MSCT scanners limited simultaneous data acquisition to 4 slices. Four detector "rows" corresponding to the 4 simultaneously collected slices fed data into 4 parallel data "channels," so that these 4-slice scanners were said to possess 4 data channels. These 4-slice scanners, however, were quite flexible with regard to how detector rows could be configured; groups of detector elements in the *z*-direction could be electronically linked to function as a single, longer detector, thus providing much flexibility in the slice thickness of the 4 acquired slices. Examples of detector configurations used with the 4 channels are illustrated in Figure 2.5 for 2 versions of 4-slice MSCT detectors: one based on the detector design described earlier (16 rows of 1.25-mm elements) and the other based on an "adaptive array" consisting of detector elements of different sizes (other detector designs were used by other manufacturers) (Flohr TG et al 2005).

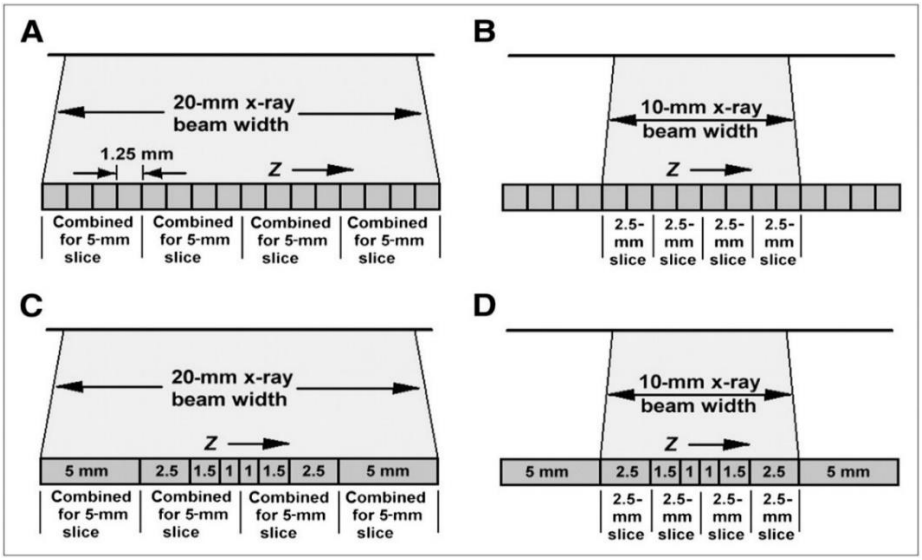

Fig (2.5) shows the Flexible use of detectors in 4-slice MSCT scanners. (A) Groups of four 1.25-mm-wide elements are linked to act as 5-mm-wide detectors. (B) Inner 8 elements are linked in pairs to act as 2.5-mm detectors. (C) Inner, adaptive-array elements are linked to act as 5-mm detectors (1 + 1.5 + 2.5) and, together with outer, 5-mm elements, yield four 5-mm slices. (D) The 4 innermost elements are linked in pairs to form 2.5-mm detectors (1 + 1.5), which along with the two 2.5-mm detectors, collect data for four 2.5-mm slices.

Possible detector configurations for the detector design encompassing 16 rows of 1.25-mm elements for the acquisition of 4 slices are illustrated in Figures 2.5 A and 2.5 B. In Figure 2.5 A, 4 elements in a group are linked to act as a single 5-mm detector (4 × 1.25). The result is four 5-mm detectors covering a total *z*-axis length of 20 mm. When a 20-mm-wide x-ray beam is used, 4 slices with a thickness of 5 mm are acquired. The acquired 5-mm slices can also be combined into 10-mm slices, if desired. In Figure 2.5 B, 4 pairs of detector elements are linked to function as four 2.5-mm detectors (2 × 1.25). When a 10-mm-wide x-ray beam is used, four 2.5-mm slices can be acquired simultaneously. Again, the resulting 2.5-mm slices can be combined to form 5-mm slices (5-mm axial slices are generally preferred for interpretation purposes). A third possibility is to use a

5-mm-wide x-ray beam to irradiate only the 4 innermost individual detector elements for the acquisition of four 1.25-mm slices. Yet another possibility is to link elements in triplets and use a 15-mm-wide x-ray beam to acquire four 3.75-mm slices. Similarly, the individual elements of the adaptive array can be appropriately linked to acquire four 5-mm slices (Fig. 2.5 C) or four 2.5-mm slices (Fig. 2.5D). Another possibility is to use a 4-mm-wide x-ray beam (which would irradiate only part of the 1.5-mm elements) to yield four 1-mm slices. Thinner slices can be combined to form thicker slices for interpretation purposes, if necessary.As data acquisition technology advanced, more data channels were provided to allow the simultaneous acquisition of more than 4 slices. An 8-channel version of the system encompassing the detector array in Figures 2.5 A and 2.5 B (introduced approximately 3 y later) could acquire eight 2.5-mm slices or eight 1.25-mm slices (which could be combined to form thicker slices for interpretation).

2.1.7 Sub-millimeter Slices and Isotropic Resolution:

The 4-slice and 8-slice MSCT scanners just described were also capable of acquiring ultrathin (“submillimeter”) slices (but only 2 at a time) by collimating the x-ray beam in the *z*-axis to partially irradiate the 2 innermost detector elements in the detector array. For example, for the detector array in Figure 2.5 A, if the x-ray beam is collimated to a 1.25-mm width and aligned so as to straddle and partially irradiate the 2 innermost detector elements, then 2 slices, each 0.625 mm thick, can be obtained. When images resulting from such an acquisition are reformatted into sagittal, coronal, or other off-axis images, the reformatted images exhibit spatial resolution in the *z*-direction that is essentially equal to that within the plane of the axial slices. Resolution that is (essentially) equal in all 3 directions is said to be isotropic.

Because only 2 submillimeter slices could be acquired simultaneously with these earlier MSCT scanners, this capability was not widely used because of limited *z*-axis coverage and tube heating limitations. Submillimeter scanning had to await the introduction of 16-slice scanners.

2.1.8 16-Channel (16-Slice) Scanners and More:

The installation of MSCT scanners providing 16 data channels for 16 simultaneously acquired slices began in 2002. In addition to simultaneously acquiring up to 16 slices, the detector arrays associated with 16-slice scanners were redesigned to allow thinner slices to be obtained as well. Detector arrays for various 16-slice scanner models are illustrated in Figure 2.6. Note that in all of the models, the innermost 16 detector elements along the *z*-axis are half the size of the outermost elements, allowing the simultaneous acquisition of 16 thin slices (from 0.5 mm thick to 0.75 mm thick, depending on the model). When the inner detectors were used to acquire submillimeter slices, the total acquired *z*-axis length and therefore the total width of the x-ray beam ranged from 8 mm for the Toshiba version to 12 mm for the Philips and Siemens versions. Alternatively, the inner 16 elements could be linked in pairs for the acquisition of 16 thicker slices.

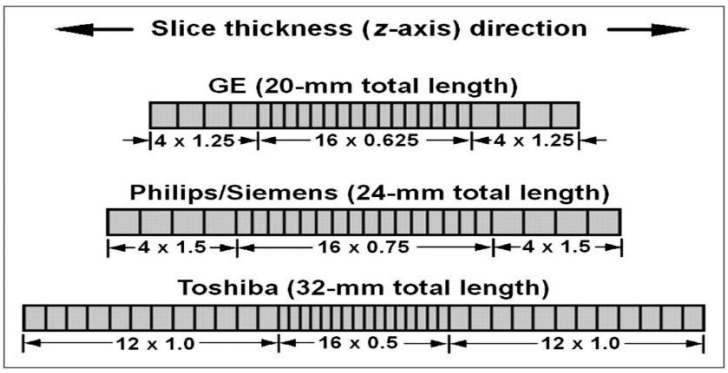

Fig (2.6) shows the diagrams of various 16-slice detector designs (in *z*-direction). Innermost elements can be used to collect 16 thin slices or linked in pairs to collect thicker slices.

During 2003 and 2004, MSCT manufacturers introduced models with both fewer than and more than 16 channels. Six-slice and 8-slice models were introduced by manufacturers as cost-effective alternatives. At the same time, 32-slice and 40-slice scanners were being introduced (Lewis M et al 2008).

By 2005, 64-slice scanners were announced, and installations by most manufacturers began. Detector array designs used by several manufacturers are illustrated in Figure 2.7 . The approach used by most manufacturers for 64-slice detector array designs was to lengthen the arrays in the *z*-direction and provide all submillimeter detector elements: 64 × 0.625 mm (total *z*-axis length of 40 mm) for the Philips and GE Healthcare models and 64 × 0.5 mm (total *z*-axis length of 32 mm) for the Toshiba model. The design approach of Siemens was quite different. The detector array of the Siemens 32-slice scanner (containing 32 elements each 0.6 mm long, for a total *z*-axis length of 19.2 mm) was combined with a "dynamic-focus" x-ray tube for the simultaneous acquisition of 64 slices. This x-ray tube could electronically—and very quickly shift the focal spot location on the x-ray tube target so as to emit radiation from a slightly different position along the *z*-axis. Each of the 32 detector elements then collected 2 measurements (samples), separated along the *z*-axis by approximately 0.3 mm. The net result was a total of 64 measurements (32 detectors × 2 measurements per detector) along a 19.2-mm total *z*-axis field of view (this process is referred to in Siemens literature as "Z-Sharp" technology) (Lewis M et al 2008).

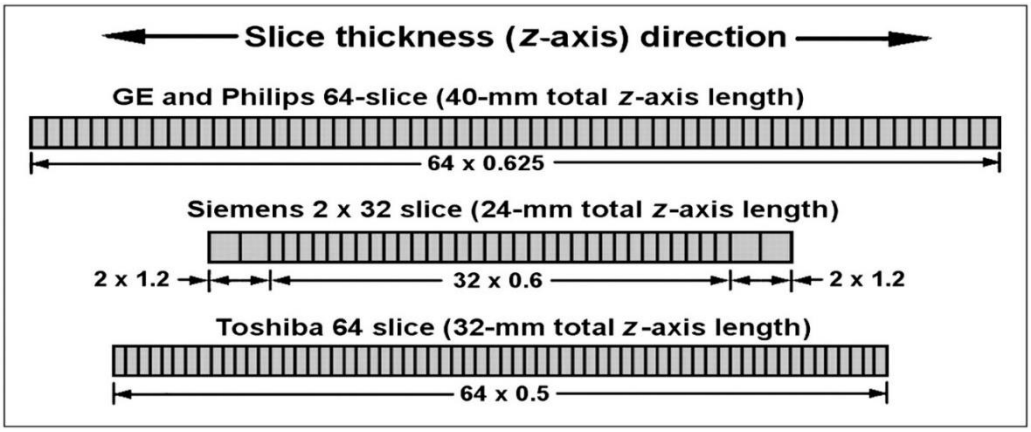

Fig (2.7) show the diagrams of various 64-slice detector designs (in *z*-direction). Most designs lengthen arrays and provide all submillimeter elements. Siemens scanner uses 32 elements and dynamic-focus x-ray tube to yield 2 measurements per detector.

In the preceding examples, in addition to the simultaneous acquisition of more slices, MSCT x-ray beam widths can be considerably wider than those for SSCT. Sixteen-slice MSCT beam widths are up to 32 mm; 64-slice beams can be up to 40 mm wide; and even wider beams are used in systems currently under development or in clinical evaluation. A possible consequence is that more scatter may reach the detectors, compromising low-contrast detection. Generally, however, the anti-scatter septa traditionally used with third-generation CT scanners can be made sufficiently deep to remain effective with MSCT. An example of a section of a 16-slice detector with the associated scatter removal septa is shown in Figure 2.8.

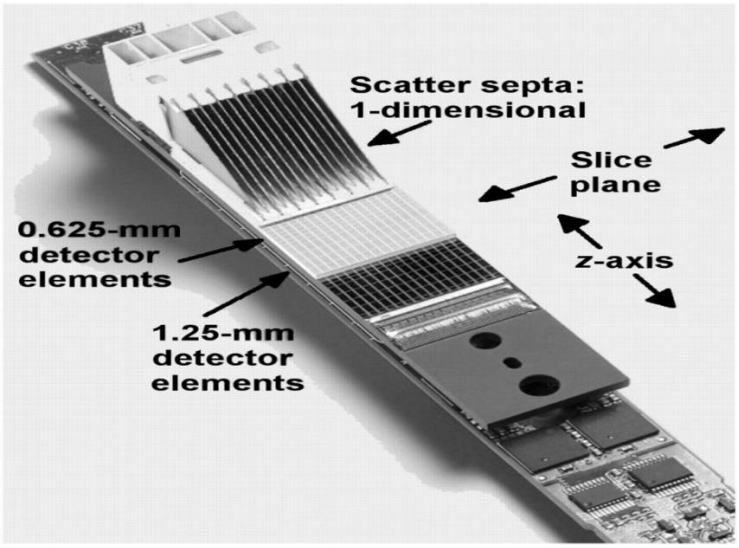

Fig (2.8) shows the Section of 16-slice detector with scatter removal septa. Septa are sufficiently deep to eliminate nearly all scatter. Note smaller elements (0.625 mm, in this example) in center of array and larger (1.25-mm) outer elements. Also note dead spaces (lighter lines) between elements.

2.2 Multi Slice Computed tomography Concepts: Differences between Multi Slice Computed tomography and Single Slice Computed tomography:

Before the further development of MSCT technology is described, certain concepts that are associated with MSCT and that may differ fundamentally from those associated with SSCT are addressed. One of these concepts is the

relationship between slice thickness and x-ray beam width. Another involves the notion of cone beam effects.

2.2.1 Multi Slice Computed Tomography Slice Thickness and X-Ray Beam Collimation:

In SSCT, slice thickness is determined by pre-patient and possibly post-patient x-ray beam collimators. Generally, the x-ray beam collimation was designed such that the *z*-axis width of the x-ray beam at the isocenter (i.e., at the center of rotation) is the same as the desired slice thickness. (The x-ray beam width, usually defined as the full width at half maximum [FWHM] of the *z*-axis x-ray beam intensity profile.

In MSCT, however, slice thickness is determined by detector configuration and not x-ray beam collimation. For example, the 4 slices in Figure 2.5A are each 5 mm thick because they are acquired by 5-mm detectors (formed by linking four 1.25-mm detector elements). The 4 slices in Figure 2.5 B are 2.5 mm thick because they are acquired by 2.5-mm detectors (formed by linking two 1.25-mm elements). Because it is the length of the individual detector (or linked detector elements) acquiring data for each of the simultaneously acquired slices that limits the width of the x-ray beam contributing to that slice, this length is often referred to as detector collimation. In Figures 2.5A and 2.5 C, the detector collimation is 5 mm. In Figures 2.5 B and 2.5 D, the detector collimation is 2.5 mm. The actual x-ray beam collimation is not directly involved in determining slice thickness, other than that the "total" *z*-axis beam collimation should be equal to the total thickness of the 4 slices, for example, 20 mm in Figure 2.5 A or 10 mm in Figure 2.5 B (that this is not necessarily true is discussed in the MSCT dosimetry section later (Goldman LW. 2007).

2.2.2 Cone Beam Effects in Multi Slice Computed Tomography:

Cone beam effects in CT are associated with the divergent nature of the x-ray beam emitted from the x-ray tube. This divergence means that the *z*-axis of the x-ray beam is somewhat wider when it exits the patient than when it entered the patient.

In SSCT, the main consequence of x-ray beam divergence is the potential for partial-volume streaking, discussed in the second article in this series (*6*) and reviewed here. During a 360° rotation, the same path (or nearly the same path) of x-rays through the patient is measured twice, but with x-rays traveling in opposite directions, for example, once with the tube above the patient and detectors below and later on during the rotation with the tube below the patient and the detectors above (these are referred to as parallel opposed rays or conjugate rays). Because of beam divergence, however, the cone-shaped x-ray beam samples slightly different tissue volumes in each direction (Fig. 2.9 A), potentially leading to data inconsistencies and streak artifacts. The thicker the slice (the wider the x-ray beam), the more pronounced the divergence and the more likely it is that parallel opposed ray measurements will be inconsistent.

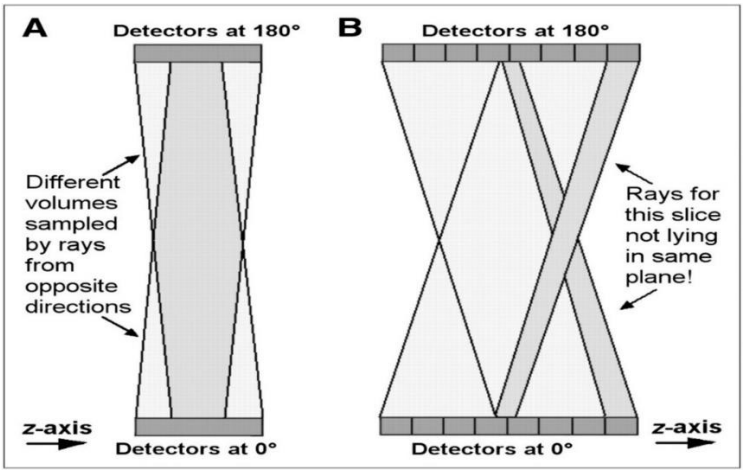

Fig (2.9) shows the cone beam effects in SSCT and MSCT. (A) In SSCT, divergent, cone-shaped x-ray beam irradiates different tissues yielding different attenuation measurements for parallel opposed rays, sometimes causing streaking for thicker slices. (B) Wider beams of MSCT accentuate cone beam shape and lead to rays that do not even lie within same plane. Cone beam reconstruction algorithms are generally required. opp. = opposite.

Cone beam effects are more severe in MSCT. Consider the MSCT configuration in Figure 2.9B, collecting data for eight 2.5-mm slices (total beam width of 20 mm). Note that the measurements obtained with the outermost detector (shading in Fig. 2.9B) from opposite sides of the patient not only sample different tissues but also do not even lie within the same slice (Flohr TG. 2005).

With 4-slice scanners, the total x-ray beam width was sufficiently narrow (e.g., 5 mm wide for four 1.25-mm slices) or else the slices were sufficiently thick (four 5-mm slices) that cone beam effects were tolerable and conventional filtered back projection reconstruction was still usable. However, MSCT scanners of later generations, which collected more and thinner slices, required the development of alternate cone beam reconstruction algorithms (which are beyond the scope of this article). Because of cone beam effects, some MSCT scanners with 16 channels or more only allow the simultaneous acquisition of the maximum number of slices (e.g., 16 slices by a 16-channel scanner) during helical scans and prevent such acquisitions during axial (non-helical) scans (Flohr TG. 2005).

2.2.3 Helical Multi Slice Computed Tomography:

Helical scanning with MSCT scanners is conceptually identical to that with SSCT scanners; rotation and table movement occur simultaneously with continuous data acquisition. However, certain terminology, along with peculiarities associated with helical pitch selection and helical slice reconstruction, tends to cause confusion. A discussion of the concept of helical pitch follows.

2.2.4 Definition of Pitch Revisited:

As originally defined for SSCT, helical pitch was calculated as table movement per rotation divided by slice thickness. For example, with a slice thickness of 5 mm and a table movement of 7.5 mm per rotation, pitch would be 1.5. Because slice thickness and x-ray beam width are equivalent in SSCT, the value for pitch conveyed important information about the x-ray beam; a pitch of 1.0 meant that the x-ray beams from adjacent rotations were essentially contiguous .Pitches of greater than 1 implied gaps between the x ray beams from adjacent rotations. Pitches of less than 1 implied x-ray beam overlap (and thus double irradiation of some tissue) and so were not clinically used.

Applying this definition to MSCT creates confusion and tends to obscure important information. For example, a 4-slice MSCT helical scan with 15 mm of table movement per rotation and a 20-mm-wide x-ray beam (to acquire four 5-mm slices) would yield the following pitch calculation based on the earlier definition:

PITCH

$$\text{Pitch} = \frac{\text{Table increment per gantry rotation (mm)}}{\text{Beam collimation* (mm)}}$$

* **Single-slice scanner:**

Beam collimation = slice thickness

* **Multislice scanner:**

Beam collimation ≠ slice thickness

So it equal 15 mm/5 mm = 3.0. This calculation does not immediately convey the fact that although the pitch is much greater than 1, there is clearly x-ray beam overlap, because the total width of the x-ray beam is 20 mm and the table is moving only 15 mm per rotation. To address this situation, a new definition of

pitch was adopted. In this definition, the denominator is replaced with the total thickness of all of the simultaneously acquired slices; that is, if *n* slices each of slice thickness T are acquired, then the total width is *n* × T, and the new pitch definition is as follows: pitch = table movement per rotation/(*n* × T) (beam pitch). Because the original definition is still occasionally referenced, the new pitch definition in the latter equation is called "beam pitch." The original definition is now referred to as "detector pitch," on the basis of the idea that slice thickness (in the denominator of the original definition) in MSCT is determined by detector configuration. With the new definition, beam pitch for the example just given would be calculated as follows: pitch = table movement per rotation/(*n* × T) = 15 mm/(4 × 5 mm) = 0.75. Because beam pitch conveys similar information for MSCT as the original definition did for SSCT, it is the preferred definition in most situations (McCollough C. 1999).

2.2.5 Pitch and z sampling in Helical Multi Slice Computed Tomography:

Clinical pitch selection in SSCT was generally straightforward. Typically, only 2 pitches were commonly used: pitch = 1 for best quality and pitch = 1.5 when more *z*-axis coverage was needed in a shorter time (because of either total scan time or x-ray tube heating constraints). Pitches of less than 1 were not used. In contrast, commonly used beam pitches in MSCT may seem odd (e.g., 0.9375, 1.125, or 1.375) and are very often less than 1. Before helical pitch in MSCT is discussed.

Because of continuous table movement, no specific slice position along the *z*-axis actually contains sufficient data (i.e., transmission measurements along ray paths through the slice at sufficient locations and angles) to reconstruct an image. Rather, required measurements are estimated by interpolation between the nearest measurements above and below the slice plane that are at the same relative position and angle. The distance along the *z*-axis between these measurements that is available for interpolation is referred to here as the *z*-

spacing. Interpolated data may be inaccurate if anatomy changes significantly within the *z*-spacing, leading to streak or shading artifacts. Helical interpolation artifacts often appear as (and are referred to as) "windmill" artifacts, because when the helical images are paged through quickly, the streak or shading artifacts seem to rotate like the vanes of a windmill. The likelihood and severity of helical artifacts increase with increasing *z*-spacing, because anatomy is more likely to change abruptly over distance. Increasing pitch (to reduce either scan time or x-ray tube heating) increases distance between interpolated measurements, so that the likelihood of helical artifacts increases.

In helical SSCT, slice data are interpolated between equivalent rays separated by a full rotation (360° apart) or between parallel opposed rays (180° apart). These 2 interpolation schemes are referred to as 360° linear interpolation (360° LI) and 180° linear interpolation (180° LI), respectively. Because parallel opposed rays in SSCT interleave those separated by 360°, *z*-spacing for 180° LI averages half that for 360° LI provides clarification of this statement). Because of its smaller *z*-spacing and therefore reduced helical artifacts, 180° LI is generally preferred over 360° LI. *z*-Spacing in helical SSCT is minimized by use of 180° LI and a pitch of 1 (assuming that pitches of less than 1 are avoided), in which case the average *z*-spacing equals d/2, where d is the slice thickness (Fig. 2.10 A).

In MSCT, 180° LI and a pitch of 1 does not improve *z*-spacing, as demonstrated by the 4-slice example in Figure 2.10 B. With detector collimation represented as "d," the detectors move relative to the patient by 4d (4 slice thicknesses) in one full 360° rotation. After a half rotation (180°), the detectors move 2D. Unlike the situation in SSCT, 180° opposed rays now duplicate, rather than interleave, those separated by a full rotation, resulting in a *z*-spacing equal to d. Suppose, instead, that a value of 3d (3 slice thicknesses) is used (Fig. 2.10 C); then, 180° opposed rays interleave those 360° apart and provide a *z*-spacing of d/2, equivalent to that achieved in SSCT with a pitch of 1 and the same slice thickness. A "rule" for this particular scheme is to overlap one detector width (one slice thickness). For the 4-slice example, this corresponds to a pitch of 3/4 = 0.75; for a 16-slice scanner, the pitch is 15/16 = 0.9375; and for a 64-slice scanner, the pitch is 63/64 = 0.9844. Note that such pitches move closer to 1 (smaller fraction of beam overlap) as the number of simultaneously acquired slices increases.

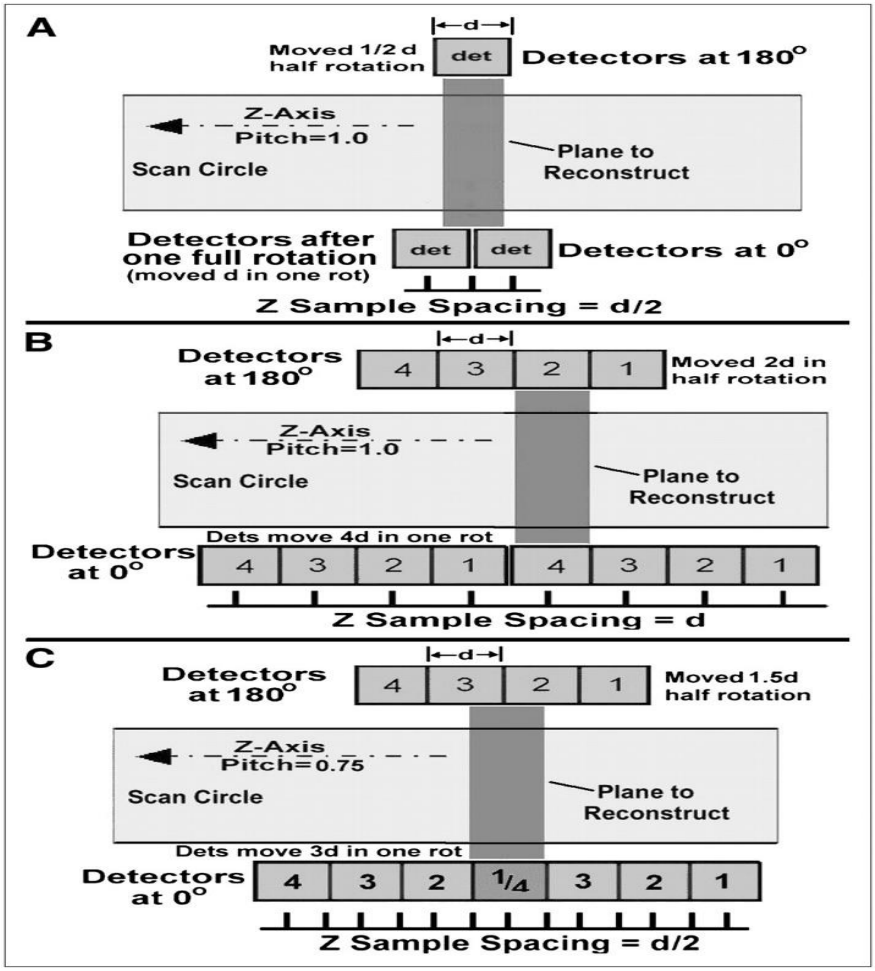

Fig (2.10) shows the *z*-Spacing in helical CT. (A) Minimum *z*-spacing equal to d/2 (d = slice thickness) is achieved in SSCT with pitch of 1 and interpolation between interleaved parallel opposed rays. (B) With pitch of 1 in MSCT, parallel opposed rays overlap rather than interleave, giving *z*-spacing equal to d. (C) *z*-Spacing equivalent to that in SSCT is achieved with pitch that overlaps one slice thickness but results in double irradiation of some tissue. Reduced *z*-spacing can also be achieved with other pitches. det = detector; rot = rotation.

2.2.6 Selection of Helical Multi Slice Computed Tomography Pitch and Data Interpolation:

Although illustrating why MSCT helical pitches may seem odd or may be less than 1, the "one-detector overlap" method is not necessarily optimal or preferred. Some MSCT scanner manufacturers recommend alternative pitch strategies, whereas still others maintain that with appropriate interpolation procedures, all (reasonable) pitches are equally good. The helical scans shown in Figure 2.11 help clarify these differences and highlight an important distinction between SSCT and MSCT data interpolation. If a 4-slice scanner uses a detector configuration of 4 × 5 mm to acquire four 5-mm-thick slices (Fig 2.11A), then slice interpolation proceeds as described earlier (usually with 180° LI), preferably with a pitch providing a smaller *z*-spacing (such as the one-detector overlap mentioned earlier) to reduce interpolation artifacts. In Figure 2.11B, with a detector collimation of 4 × 1.25 mm, 13 detector samples lie completely or partially within the 5-mm slice plane to reconstruct (depending on the slice position relative to the overlapping detectors, 11–13 samples may lie within the slice plane). It is clear that this example no longer involves a simple interpolation between the 2 nearest points but rather requires an appropriate combination of all measurements lying within the slice. With appropriate weighting, these measurements may be combined to form a 5-mm-thick slice measurement with a well-shaped beam profile. This process is referred to as "*z* filtering." With a pitch of 1 rather than 0.75, *z*-spacing increases from 0.625 mm (i.e., d/2) to 1.25 mm (i.e., d) and leads to only minor degradation of the slice profile shape and increased helical artifacts. For 16-slice scanners (and more), the detector collimation during helical scans is 1.5 mm or less (depending on the model and beam width), with correspondingly small differences in the slice profile shape versus pitch. (Wang G. et al 1999)

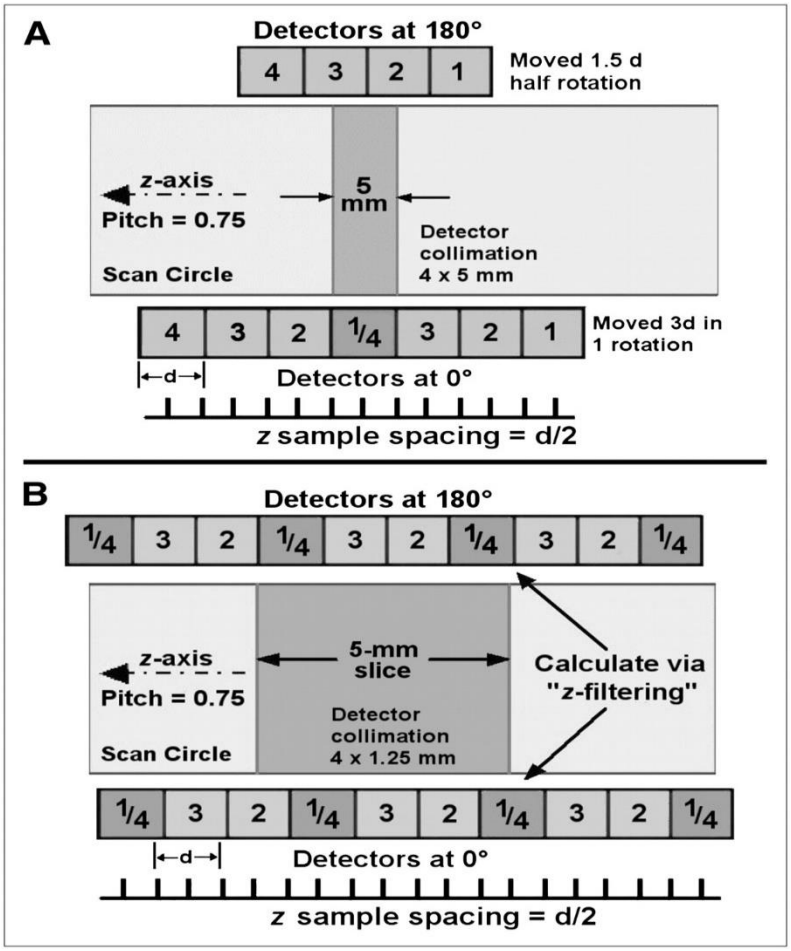

Fig (2.11) shows the *z* Filtering.(A) For MSCT scans configured to acquire thicker slices (5 mm), slices are interpolated as for SSCT. (B) For MSCT scans with small detector collimation, numerous measurements are obtained within slice plane (up to 13, in this example) to form thicker slices. Combining many measurements to form thicker slices is referred to as *z* filtering.

2.2.7 Helical Multi Slice Computed Tomography Pitch and mAs:

Low contrast sensitivity (the ability to resolve low-contrast structures) depends on CT image noise. CT image noise originates primarily from quantum mottling, which depends on the number of x-ray photons contributing to the image (the appearance of image noise also depends on the sharpness of the reconstruction filter used). To understand how various factors affect CT image noise, it is easiest to consider how many x-ray photons contribute to each detector

measurement. Relevant factors include kVp (with higher kVp, more x-rays penetrate the patient to reach the detectors), slice thickness (the detectors collect more photons over thicker slices), x-ray tube mA (a higher x-ray intensity increases the number of detected x-rays proportionally), and rotation time (faster rotation corresponds to shorter detector sampling times). The last 2 factors are often taken together as mAs (see the second article in this series for a more complete discussion) (Goldman LW . 2008).

Helical SSCT slices are reconstructed from data interpolated between the 2 nearest parallel ray measurements (usually with 180° LI). Therefore, the number of x-ray photons contributing to each interpolated sample (and therefore to reducing image noise) is a linear combination of 2 detector measurements, regardless of pitch. That is, helical SSCT image noise is unaffected by pitch (*9*). (Note, however, that the interpolation algorithm does affect image noise; fewer rays contribute to images when 180° LI is used than when 360° LI is used, so that 180° LI images are somewhat noisier). Pitch does affect image noise in helical MSCT if slice measurements are formed from many detector samples. For example, the 5-mm slice in Figure 8B is formed from a combination of 11–13 detector measurements. If the average x-ray flux reaching each detector element is *n*, then the number of x-ray photons contributing to the calculated (*z*-filtered) sample is between 11*n* and 13*n*. In comparison, a pitch of 1.5 and a detector collimation of 4 × 1.25 mm results in only 5–7 detector measurements lying within the 5-mm slice plane and thus contributing to each slice sample. For the same average detector flux *n* as that used in the earlier example, the number of contributing x-ray photons is 5*n*–7*n*. That is, fewer x-ray photons contribute to each calculated slice sample for larger pitches, leading to noisier images.

In general, the number of photons contributing to images decreases linearly with helical MSCT pitch if the same x-ray technique settings (kVp and mAs) are

used. As discussed later in this article, with the same x-ray technique factors, patient radiation dose (CT volume dose index [$CTDI_{vol}$]) also decreases linearly with pitch (in effect, the same amount of energy is spread over more tissue in the *z*-direction). Therefore, a practice adopted by some manufacturers is to specify "effective"mAs(mAs_{eff}), calculated as

$$\mathbf{mAs_{eff} = mAs/pitch}$$

rather than actual mAs, during examination prescription. mAs_{eff} is chosen to maintain the same level of image noise regardless of selected pitch. For example, with 1-s rotation times, a mAs_{eff} of 240 uses 240 mA with a pitch of 1 (mAs_{eff} = 240/1 = 240) but uses 300 mA with a pitch of 1.25 (mAs_{eff} = 300/1.25) and 200 mA with a pitch of 0.83(mAs_{eff} = 200/0.83). (Goldman LW 2008)

2.3 Multi Slice Computed Tomography Radiation Dosimetry:

Although axial and helical MSCT involves a more complex data collection process, measuring and specifying patient radiation doses in MSCT are no different from in SSCT. For both axial and helical dosimetry purposes, detector collimation is ignored and an MSCT scanner is treated as a single-slice scanner with a slice thickness equal to the full collimated x-ray beam width. For example, an MSCT scan with a detector collimation of 4 × 2.5 mm (total beam width of 10 mm) would be treated for dosimetry purposes as an SSCT scan with a slice thickness of 10 mm (see the second article in this series for a complete discussion of CT dosimetry). For axial scans, therefore, the weighted CTDI [$CTDI_w$] for a detector collimation of 4 × 2.5 mm (the slices from which may be combined to form 10-mm slices) is equivalent in principle to that of a 10-mm SSCT slice. Similarly, the $CTDI_{vol}$ for helical scans is obtained from axial $CTDI_w$ measurements at the same beam collimation by dividing the axial $CTDI_w$ by the pitch.

There are, however, certain factors that reduce the dose efficiency of MSCT relative to SSCT. In addition, certain MSCT practices that were uncommon or nonexistent in SSCT may lead to increased patient radiation doses. These factors and issues are described in the following discussion.

2.3.1 Multi Slice Computed Tomography Dose Efficiency:

Dose efficiency refers to the fraction of x-rays that reach the detectors and that are actually captured and contribute to image formation. Dose efficiency has 2 components: geometric efficiency and absorption efficiency. Absorption efficiency refers to the fraction of x-rays that enter active detector areas and that are actually absorbed (captured). Absorption efficiencies are similar for all SSCT and MSCT scanners that have solid-state detectors. Geometric efficiency refers to the fraction of x-rays that exit the patient and that enter active detector areas.

Two aspects of MSCT reduce its geometric dose efficiency relative to that of SSCT. The first is the obvious necessity for dividers between individual detector elements along the *z*-axis, which create dead space that did not exist within SSCT detectors in the *z*-direction (there is, of course, dead space from detector dividers within the slice plane for both SSCT and MSCT). These dividers are visible in Figure 2.8 as the thin, lighter lines between the small detector elements. Depending on detector design and element size, dead space associated with the dividers can represent up to 20% of the detector surface area. That is, up to 20% of x-rays exiting the patient will strike dead space and not contribute to image formation. Because these dividers must satisfy anti–cross talk and physical separation requirements, divider width generally remains unchanged as detector elements are made smaller (compare the dividers between the 0.625-mm elements and the 1.25-mm elements in (Fig 2.8). Therefore, the dividers represent a larger fraction of detector surface area for smaller elements, leading

to lower geometric efficiency. Reducing detector element width from 1.25 mm to 0.635 mm or from 1.5 mm to 0.75 mm approximately doubles the amount of dead space. Geometric efficiency loss is fixed by MSCT detector design and cannot be recovered (Hsieh J. 2001).

The second factor that reduces MSCT geometric efficiency is associated with the x-ray beam width. In SSCT, the beam width is taken to be the *z*-axis dose profile width measured at the isocenter (i.e., at the axis of rotation) between profile points corresponding to 50% of the maximum intensity (referred to as the FWHM). A collimator is designed such that the profile FWHM corresponds to the desired slice thickness. Figure 2.12A illustrates such a dose profile for a 10-mm-wide beam used to irradiate an MSCT detector collimation of 4 × 2.5 mm (to acquire four 2.5-mm slices). Four sections of this profile are shaded to emphasize the x-ray flux contributing to each of the 4 slices. Note that the 2 outer slices receive fewer x-rays and therefore exhibit more quantum mottling than do the 2 inner slices. This undesirable situation arises because the 2 outer slices are partially irradiated by the dose profile "edges" (which correspond to the beam penumbra). Providing equivalent radiation to all 4 slices requires that the x-ray beam be widened such that all 4 slices are irradiated by the inner, non-penumbra region, as illustrated in Figure 2.12 B. In effect, the penumbra regions that contributed to SSCT images cannot be used in MSCT and must be discarded (Hsieh J. 2001).

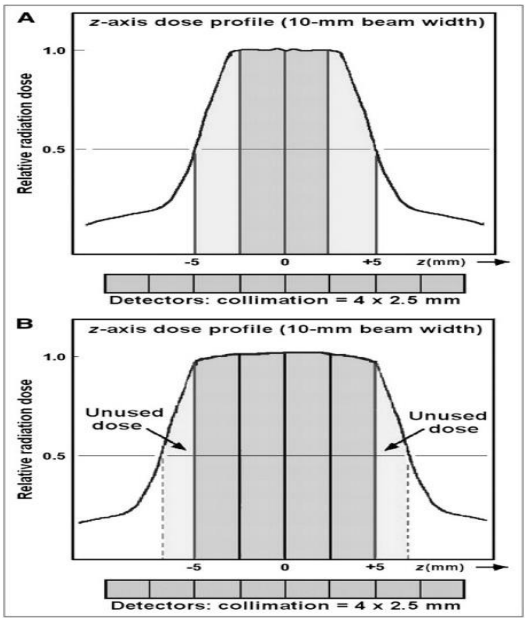

Fig (2.12) shows the Geometric dose efficiency. (A) If MSCT detectors configured to acquire four 2.5-mm slices are irradiated with 10-mm-wide x-ray beam, as specified for SSCT, outer 2 slices will receive lower intensity and yield higher image noise. (B) To compensate, MSCT beams are widened to use only inner, non penumbra regions. Penumbra regions that were partially used in SSCT are discarded in MSCT, leading to reduced dose efficiency.

The size of the beam penumbra is related to the collimator design and the focal spot size and changes only moderately at different beam widths. As a result, the fractional loss of dose efficiency associated with the discarded penumbra becomes smaller for larger beam widths, because the penumbra represents a smaller fraction of the total x-ray beam width. A consequence is that CTDI values in MSCT are higher for smaller beam collimation values (Table 1). In comparison, CTDI values in SSCT are nearly independent of slice thickness (and thus beam width, as defined earlier), except in certain cases of thin slices (~1 mm) for which the beam width deviates from the earlier definition. As beams become even wider for higher-slice-count scanners (currently up to 40 mm for

64-slice scanners), the geometric efficiency loss associated with the penumbra becomes less and less of a factor.

Table 2.1 Demonstrate the $CTDI_w$ vs. Beam Collimation

$CTDI_w$ vs. Beam Collimation

Total beam collimation (mm)	Detector configuration	$CTDI_w$ relative to 10-mm beam
5	4 × 1.25 mm	1.22
10	4 × 2.5 mm	1.00
15	4 × 3.75 mm	0.93
20	16 × 1.25 mm	0.89
40	16 × 2.5 mm	0.83

Because discarded penumbra represents smaller fraction of total beam width, CTDI values decrease with increasing beam widths (combined data from GE Healthcare 4-slice and 64-slice MSCT scanners)

2.3.2 Variations within the Scan Plane:

Projectional radiographic exposures are taken from one source position and the entrance skin dose is much larger than the exit skin dose, creating a large radiation dose gradient across the patient (Fig 2.13).

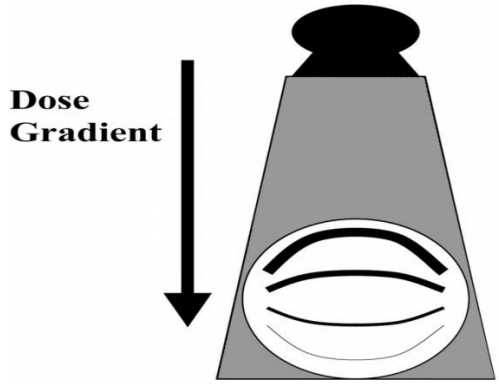

Fig (2.13) dose gradients resulting from a projectional radiographic exposure in which the source is stationary at one position. The thicker lines represent the entrance skin dose, which is much larger than the exit skin dose, represented by the thinner lines. This difference creates a linear gradient through the patient.

In contrast, the tomographic exposure of CT scans with a full 360° rotation results in a radially symmetric radiation dose gradient within the patient. That is, in a uniform circular object, such as a test phantom, all of the points at a certain radius from the center have the same (or nearly the same) radiation dose (Fig 2.14). (Michael F et al 2002).

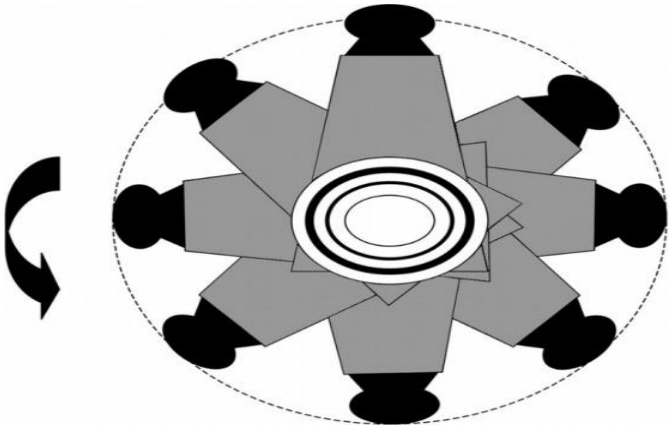

Fig (2.14) shows the Dose gradient resulting from a full 360° exposure from a CT scan. The thicker lines represent the entrance skin dose, which is much larger than the dose at the inner radius, represented by the thinner lines. This difference results in a radially symmetric radiation dose gradient within the patient.

As we shall see, the magnitude of that dose gradient (the size of the difference from center to periphery) will be affected by several factors, including the size of the object, the x-ray beam spectrum, and the attenuation of the material or tissue. (Michael F et al 2002).

For example, in a typical CT dosimetry phantom that is 32 cm in diameter and made of polymethyl methacrylate (PMMA) usually referred to as the *body phantom*—measurements of CT dose, which will be defined later, obtained at the center are typically about 50% of the measured value obtained at one of the peripheral positions. This result is illustrated in Figure 2.15, which shows the center value obtained under specific conditions to be approximately 10 mGy while the peripheral values are 20 mGy under those same conditions. (Michael F et al 2002).

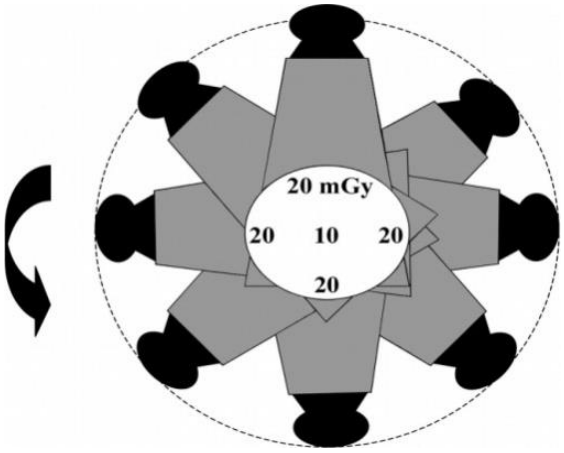

Fig (2.15) shows the typical dose measurements in a 32-cm-diameter (body) phantom from a single-detector CT scan. Values measured at the center and periphery (1 cm below the surface) positions within a polymethyl methacrylate circular dosimetry phantom demonstrate a radial dose gradient with a 2:1 ratio from periphery to center. Technical factors for the measurements were 120 kVp, 280 mA, 1-sec scan (ie, 280 mAs), and 10-mm collimation.

However, for a smaller-diameter phantom the 16-cm-diameter phantom referred to as the head phantom measured under the identical exposure conditions, the center value reading climbs to approximately 40 mGy, as do the peripheral values (Fig 2.16). This indicates that the magnitude of the difference from center to periphery is very much size dependent; it also indicates that the absolute values of the absorbed doses are size dependent.

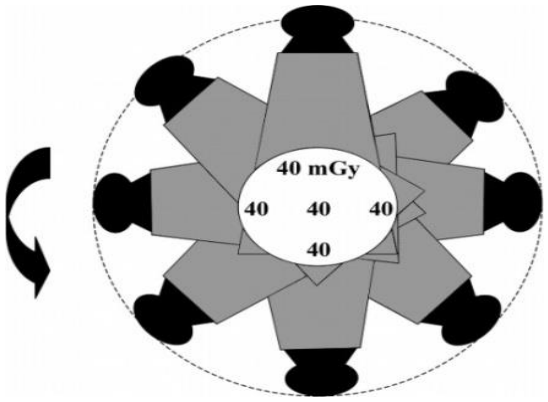

Fig (2.16) shows the typical dose measurements in a 16-cm-diameter (head) phantom from a CT scan.Values measured at the center and periphery (1 cm below the surface) positions within a polymethyl methacrylate circular dosimetry phantom demonstrate essentially no radial dose gradient. Technical factors for the measurements were 120 kVp, 300 mA, 1-sec scan (ie, 300 mAs), and 5-mm collimation.

2.3.3 Z-Axis Variations:

In addition to the variations within the scan plane, there are variations along the length of the patient or phantom. These can be characterized by the z-axis dose distribution or radiation profile (Fig2.17).

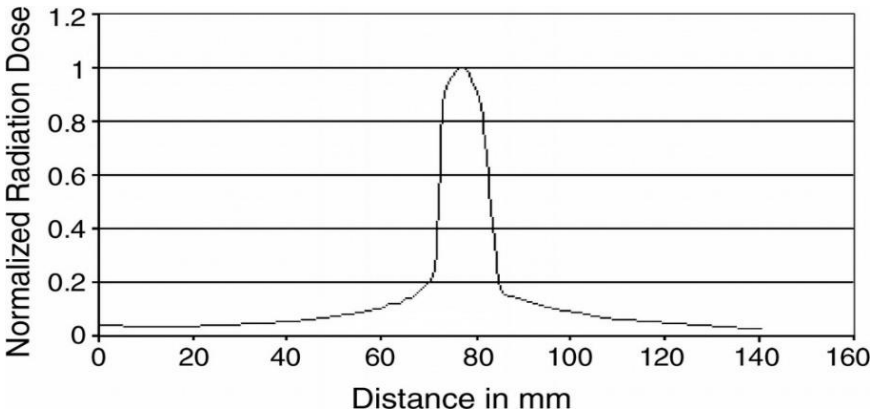

Fig (2.17) shows the Radiation profile of a full-rotation CT scan measured at isocenter. This profile is the distribution of radiation dose along the axis of the patient (the z axis) and is known as *D* (z).

This is the distribution of absorbed dose along the axis of the patient due to a single axial scan (a full rotation at one table position). The radiation profile is not limited to the primary area being imaged, and there are tails to this distribution from the non-ideal collimation of the x-ray source and from scatter of photons within the object being exposed. When multiple adjacent scans are performed, the tails of the radiation profiles from adjacent scans can contribute to the absorbed dose outside of the primary area being imaged. If these tails are significant and are non-zero at some distance from the location of the originating section, then these contributions can add up, creating additional absorbed dose in the primary area being imaged.

That is, the radiation dose in a specific section consists of the sum of contributions to that section when that area is the primary area being imaged as

well as the contributions from the tails of radiation profiles from adjacent sections when other locations are the primary area being imaged. The size of the contributions from adjacent sections is very directly related to the spacing of sections and the width and shape of the radiation profile.

To account for the effects from multiple scans, several dose descriptors were developed. One of the first was the Multiple Scan Average Dose (MSAD) descriptor (Shrimpton PC 1998). This is defined as the average dose resulting from a series of scans over an interval *I* in length:

Following this was the Computed Tomography Dose Index (CTDI). This was defined as the radiation dose, normalized to beam width, measured from 14 contiguous sections:

This index was suggested by the Food and Drug Administration and incorporated into the Code of Federal Regulations (Federal Register 1984).

However, to be measured according to the definition, only 14 sections could be measured and one had to measure the radiation dose profile typically done with thermoluminescent dosimeters (TLDs) or film, neither of which was very convenient. Measurements of exposure could be obtained with a pencil ionization chamber, but its fixed length of 100 mm meant that only 14 sections of 7-mm thickness could be measured with that chamber alone. To measure CTDI for thinner nominal sections, sometimes lead sleeves were used to cover the part of the chamber that exceeded 14 section widths.

To overcome the limitations of CTDI with 14 sections, another radiation dose index ($CTDI_{100}$) was developed. This index relaxed the constraint on 14 sections and allowed calculation of the index for 100 mm along the length of an entire

pencil ionization chamber, regardless of the nominal section width being used. This index is therefore defined as follows (EUR 16262 en, may 1999):

2.3.4 Factors That Influence Radiation Dose from CT Section:

In general, there are some factors that have a direct influence on radiation dose, such as the x-ray beam energy (kilovolt peak), tube current (in milliamperes), rotation or exposure time, section thickness, object thickness or attenuation, pitch and/or spacing, dose reduction techniques such as tube current variation or modulation, and distance from the x-ray tube to isocenter. In addition, there are some factors that have an indirect effect on radiation dose those factors that have a direct influence on image quality, but no direct effect on radiation dose; for example, the reconstruction filter. Choices of these parameters may influence an operator to change settings that do directly influence radiation dose. These factors are discussed in this section.(Nagel HD2000)

2. 3.4.1 Beam Energy:

The energy of the x-ray beam has a direct influence on patient radiation dose. This is selected by the operator (technologist) when the kilovolt peak is chosen for the scan. However, it is also influenced by the filtration selected for the scan. On some scanners, the selection of filtration is explicit; for others, it is implied (eg, by selection of the scan field of view [SFOV]). The influence of beam energy is shown in Table 1. When all other technical parameters are held constant and the kilovolt peak is increased on a single-detector CT scanner, the $CTDI_w$ values also increase for both the head and body CTDI phantoms. For example, when the kilovolt peak was increased from 120 to 140 on a CT/i scanner (GE Medical Systems, Milwaukee, Wis), the $CTDI_w$ increase was 37.5% for the head phantom and 39% for the body phantom.

Table (2.2) demonstrate the Changes in $CTDI_w$ in Head and Body Phantoms as a Function of Kilovolt Peak

Beam Energy (kVp)	$CTDI_w$ in Head Phantom (mGy)	$CTDI_w$ in Body Phantom (mGy)
80	14	5.8
100	26	11
120	40	18
140	55	25

Effective dose is becoming a very useful radiation quantity for expressing relative risk to humans both patients and other personnel .it is actually a simple and ver logical concept. T takes into account the specific organs and area of the body that are exposed. The point is that all the parts of the body and organs are not equally sensitive to the possible adverse effects of radiation, such as cancer induction and mutations.

For the purpose of determining effective dose, the different areas and organs have been assigned tissue weighting factor (W_T) values. For a specific organ or body area the effective dose is:

Effective Dose (Gy) = Absorbed Dose (Gy) x W_T:

If more than one area has been exposed, then the total body effective dose is just the sum of the effective doses for each exposed area. It is a simple as that. Now let's see why effective dose is such a useful quantity. There is often a need to compare the amount of radiation received by patients for different types of x-ray procedures, for example, a chest radiograph and a CT scan. The effective dose is the most appropriate quantity for doing this. Also, by using effective dose it is

possible to put the radiation received from diagnostic procedures into perspective with other exposures, especially natural background radiation.

It is generally assumed that the exposure to natural background radiation is somewhat uniformly distributed over the body. Since the tissue weighting factor for the total body has the value of one (1), the effective dose is equal to the absorbed dose. This is assumed to be 300 mrad in the illustration.

Let's look at an illustration. If the the dose to the breast, MGD, is 300 mrad for two views, the effective dose is 45 mrad because the tissue weighting factor for the breast is 0.15 What this means is that the radiation received from one mammography procedure is less than the typical background exposure for a period of two months.

Table (2.3) tissue weighting factors UNSCEAR 2008

ORGANS	ICRP30(136) 1979	ICRP 60(13) 1991	ICRP 103(16) 2008
Gonads	0.25	0.20	0.08
Red bone marrow	0.12	0.12	0.12
colon	-	0.12	0.12
lung	0.12	0.12	0.12
Stomach	-	0.12	0.12
Breast	0.15	0.05	0.12
Bladder	-	0.05	0.04
Liver	-	0.05	0.04
Esophagus	-	0.05	0.04
Thyroid	0.03	0.05	0.04
Skin	-	0.01	0.01
Bone surface	0.03	0.01	0.01
Salivary glands	-	-	0.01
Brain	-	-	0.01
Remainder of body	0.30	0.05	0.12

2.3.5 Radiation dose units:

2.3.5.1 Common Units (USA):

Roentgen (R) The roentgen is a unit used to measure a quantity called exposure. This can only be used to describe an amount of gamma and X-rays, and only in air. One roentgen is equal to depositing in dry air enough energy to cause 2.58 x 10^{-4} coulombs per kg. It is a measure of the ionizations of the molecules in a mass of air. The main advantage of this unit is that it is easy to measure directly, but it is limited because it is only for deposition in air, and only for gamma and x rays.(UNSCEAR2000)

Rad (radiation absorbed dose) the rad is a unit used to measure a quantity called absorbed dose. This relates to the amount of energy actually absorbed in some material, and is used for any type of radiation and any material. One Rad is defined as the absorption of 100 ergs per gram of material. The unit Rad can be used for any type of radiation, but it does not describe the biological effects of the different radiations. (UNSCEAR2000)

Rem (roentgen equivalent man) the Rem is a unit used to derive a quantity called equivalent dose. This relates the absorbed dose in human tissue to the effective biological damage of the radiation. Not all radiation has the same biological effect, even for the same amount of absorbed dose. Equivalent dose is often expressed in terms of thousandths of a Rem, or mrem. To determine equivalent dose (Rem), you multiply absorbed dose (Rad) by a quality factor (Q). (UNSCEAR2000)Curie (Ci) (radioactivity) the curie is a unit used to measure a radioactivity. One curie is that quantity of a radioactive material that will have 37,000,000,000 transformations in one second. Often radioactivity is expressed in smaller units like: thousandths (mCi), one millionths (μCi) or even billionths

(nCi) of a curie. The relationship between Becquerel's and curies is: 3.7 x 10^{10} Bq in one curie. (UNSCEAR2000)

2.3.5.2 Common Units (SI) International:

Gray (Gy) The gray is a unit used to measure a quantity called absorbed dose. This relates to the amount of energy actually absorbed in some material, and is used for any type of radiation and any material. One gray is equal to one joule of energy deposited in one kg of a material. The unit gray can be used for any type of radiation, but it does not describe the biological effects of the different radiations. Absorbed dose is often expressed in terms of hundredths of a gray, or centi-grays (cGy). One gray is equivalent to 100 rads.Sievert (Sv) the sievert is a unit used to derive a quantity called equivalent dose. This relates the absorbed dose in human tissue to the effective biological damage of the radiation. Not all radiation has the same biological effect, even for the same amount of absorbed dose. Equivalent dose is often expressed in terms of millionths of a sievert, or micro-sievert (µSv) or thousandth of a sievert as a milli-sievert (mSv). One sievert is equivalent to100 rem. (UNSCEAR2000Becquerel (Bq) (radioactivity) The Becquerel is a unit used to measure a radioactivity. One Becquerel is that quantity of a radioactive material that will have 1 transformations in one second. Often radioactivity is expressed in larger units like: thousands (kBq), one millions (MBq) or even billions (GBq) of a becquerels. As a result of having one Becquerel being equal to one transformation per second, there are 3.7 x 10^{10} Bq in one (UNSCEAR2000).

Note: Radiation dose is measured in rem or sievert (or fractions of those units). Radiation dose rate is measured in dose per unit time, such as rem/hr or Sv/hr. If you have a dose rate, multiply by the amount of time present in the radiation field, to get dose.For instance 320 mrem/ hr x 6 minutes = 32 mrem dose

2.3.6 CT dose measurements:

Although computed tomography (CT) represents only a small percentage of radiologic examinations, it results in a significant portion of the effective radiation dose from medical procedures (1). With the increasing use of CT for screening procedures (2) and advances in scanner technology, the trend for increased numbers of procedures performed with this imaging modality may increase. Although CT is clearly providing many clinical benefits, the motivation to understand radiation dose in general as well as the specific concepts related to CT grows with the prevalence of this modality. (ImPACT 2007, jones et al.1993)

2.3.7 CT Dose descriptors:

The dose quantities used in projection radiography are not applicable to CT for three reasons:

First, the dose distribution inside the patient is completely different from that for a conventional radiogram, where the dose decreases continuously from the entrance of the X-ray beam to its exit, with a ratio of between 100 and 1000 to 1. In the case of CT, as a consequence of the scanning procedure that equally irradiates the patient from all directions; the dose is almost equally distributed in the scanning plane. A dose comparison of CT with conventional projection radiography in terms of skin dose therefore doesn’t make any sense.(ImPACT 2007, jones et al.1993)

Second, the scanning procedure using narrow beams along the longitudinal z-axis of the patient implies that a significant portion of the radiation energy is deposited outside the nominal beam width. This is mainly due to penumbra effects and scattered radiation produced inside the beam.(ImPACT 2007, jones et al.1993)

Third, the situation in CT is further complicated by the circumstances in which unlike in conventional projection radiography the volume to be imaged is not irradiated simultaneously. This often leads to confusion about what the dose from a complete series of e.g. 15 slices might be compared with the dose from a single slice.(ImPACT 2007, jones et al.1993)

As a consequence, dedicated dose quantities that account for these peculiarities are needed: The 'Computed Tomography Dose Index (CTDI)', which is a measure of the local dose, and the 'Dose-Length Product (DLP)', representing the integral radiation exposure associated with a CT examination. Fortunately, a bridge exists that enables to compare CT with radiation exposure from other modalities and sources; this can be achieved by the effective dose (E). So there are three dose descriptors in all, which everyone dealing with CT should be familiar with. (ImPACT 2007, jones et al.1993).

2.3.8 CT parameters that influence the radiation dose:

The radiation exposure to the patient undergoing CT examinations is determined by two factors (nagel 2007).

2.3.8.1 Computed Tomography Dose Index:

The 'Computed Tomography Dose Index (CTDI)' is the fundamental CT dose descriptor. By making use of this quantity, the first two peculiarities of CT scanning are taken into account: The CTDI (unit: Milligray (mGy) is derived from the dose distribution along a line which is parallel to the axis of rotation for the scanner (= z-axis) and which is recorded for a single rotation of the x-ray source. (Fig. 2.18)

Illustrates the meaning of this term: CTDI is the equivalent of the dose value inside the irradiated slice (beam) that would result if the absorbed radiation dose

profile were entirely concentrated to a rectangular profile of width equal to the nominal beam width N·hcol, with N being the number of independent (i.e. non-overlapping) slices that are acquired simultaneously. Accordingly, all dose contributions from outside the nominal beam width, i.e. the areas under the tails of the dose profile, are added to the area inside the slice.

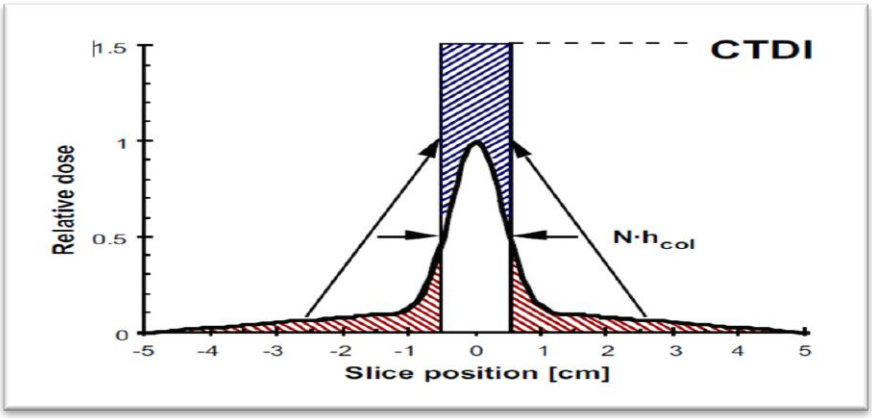

Fig (2.18) Illustration of the term ’Computed Tomography Dose Index (CTDI)’: CTDI is the equivalent of the dose value inside the irradiated slice (beam) that would result if the absorbed radiation dose profile were entirely concentrated to a rectangular profile of width equal to the nominal beam width (N·hcol.

CTDI is therefore equal to the area of the dose profile (the ‘dose profile integral’) divided by the nominal beam width. In practice, the dose profile is accumulated in a range of –50 mm to + 50 mm relative to the center of the beam, i.e. over a distance of 100 mm. The relevancy of CTDI becomes obvious from the total dose profile of a scan series with e.g. n=15 subsequent rotations (fig 2.19).the average level of the total dose profile, which is called ‘Multiple Scan Average Dose (MSAD)’ (Shope 1981),is higher than the peak value of each single dose profile. This increase results from the tails of the single dose profiles for a scan series. Obviously, MSAD and CTDI are exactly equal if the table feed TF is equal to the nominal beam width N·hcol, i.e. if the pitch factor

Is equal to 1 in general (i.e. if the pitch is not equal to 1, see fig. 2.19), the relationship between CTDI and MSAD is given by:

$$MSAD = {}^{1}/_{p}.CTDI$$

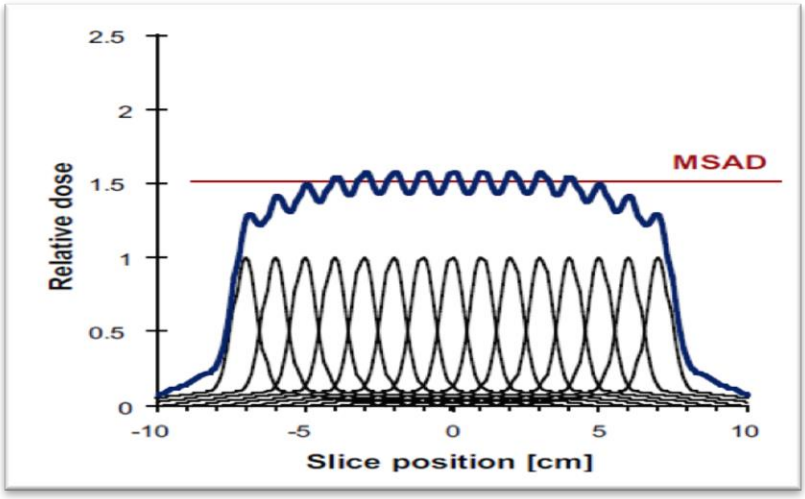

Fig (2.19) shows the Total dose profile of a scan series with n=15 subsequent rotations. The average level of the total dose profile, which is called 'Multiple Scan Average Dose (MSAD)', is equal to CTDI the table feed TF is equal to the nominal beam width N·hcol (i.e. pitch=1).

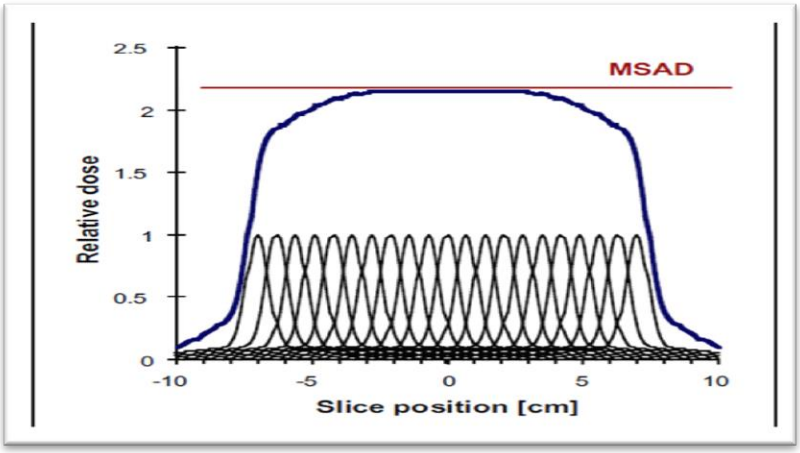

Fig (2.20) shows the Total dose profile of a scan series with n=15 subsequent rotations, scanned with pitch = 0.7, However. Due to the larger overlap, MSAD is higher than in fig. 2.20 and amounts to CTDI divided by pitch.

Each pair of CTDI (central or peripheral) can be combined into single are named weighted CTDI (CTDI*w*)

If pitch-related effects on radiation exposure are taken into account at level of local dose (i.e CTDI) already a quantity named volume CTDI (CTDI*vol*) (IEC2001)

So CTDI*vol* is the pitch-corrected CTDI*w*. Apart from the Integration length, which is limited to 100 mm, CTDIvol is practically identical to MSAD based on CTDI*w* (i.e. MSAD*w*). Since averaging includes both the cross section and the scan length, CTDI*vol* therefore represents the average dose for a given scan volume. CTDIvol is used as the dose quantity that is displayed at the operator's console of newer scanners. (Nagel 2007)

2.3.8.2 Dose-Length Product:

Dose-length product (DLP; unit: mGy·cm). DLP takes both the 'intensity' (represented by the CTDIvol) and the extension (represented by the scan length L) of an irradiation into account (fig 2.21)

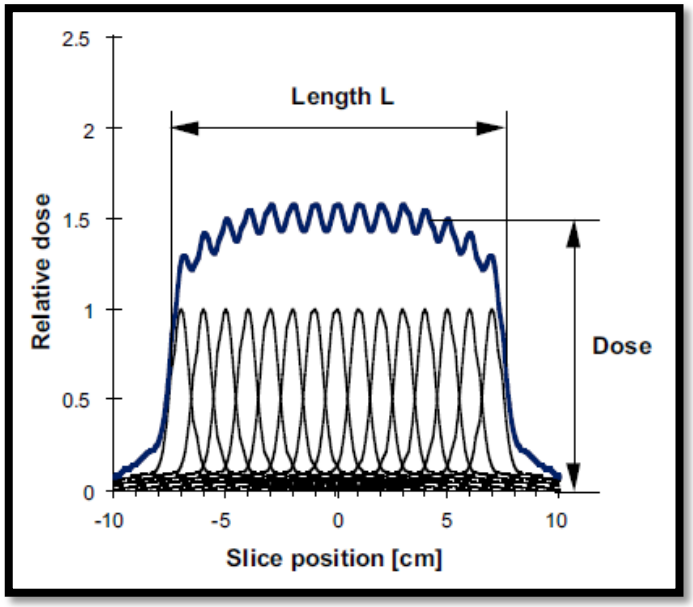

Fig (2.21) shows the Total dose profile of a scan series with n=15 subsequent rotations. The dose-length product (DLP) is the product of the height (dose, i.e. CTDIvol) and the width (scan length L) of the total dose profile and is equal to the area under the curve by the European Commission (1999).

So the dose-length product increases with the number of slices (correctly: with the length of the irradiated body section), while the dose (i.e. CTDIvol) remains the same regardless of the number of slices or length, respectively.

In fig. 2.21, the area of the total dose profile of the scan series represents the DLP. DLP is the equivalent of the dose-area product (DAP) in projection radiography, a quantity that also combines both aspects (intensity and extension) of patient exposure. In sequential scanning, the scan length is determined by the beam width N·hcol and the number n of tables feeds.

While in spiral scanning the scan length only depends on the number n of rotations and the table feed.

If an examination consists of several sequential scan series or spiral scans, the dose-length product of the complete examination (DLPexam) is the sum of the dose-length products of each single series or spiral scan.

2.1.1 Anatomy of para nasal sinuses

The par nasal sinuses are air filled spaces located within the bones of the skull & face, they are central on the nasal cavity they are four sets of paired sinuses are:

2.1.1.1 Maxillary sinus:

The maxillary sinus is the largest P.N.S and found inferior to the eyes in the maxillary bone; It is the first sinus to develop and filled with fluid at birth. The shape of the sinuses is a pyramid the natural osmium of the maxillary sinuses is located in the superior portion of the medial wall. The roof of the maxillary sinuses is the floor of the orbit. The maxillary sinuses is supplied by branches of the internal maxillary artery which include the infra orbital, alveolar, greater palatine, and spheno palatine arteries. (Ameet singh et- al, 2013).

2.1.1.2 Frontal sinus:

The frontal sinus is housed in the frontal bone superior to eyes in the forehead. The frontal sinuses are funnel. Shaped structures with Ostia located in the most dependent portion of the cavities, the posterior Wall of the frontal sinus much thinner than the anterior wall. It is supplied by sub orbital and supra orbital and subratrochlear arteries of the ophthalmic artery. (Ameet singh et- al, 2013).

2.1.1.3 Ethmccoide Sinuses

The ethmoide Sinuses forming several distinct air cells between the eyes. The shaped like pyramids and divided by thin septa, The ethmoide labyrinth may extend a bove the orbit, lateral and superior to the sphenoid ,above the frontal sinuses and into the roof of the maxillary sinuses and supplied by the anterior and posterior ethmoidal arteries. (Ameet singh et- al 2013).

2.1.1.4 Sphenoid sinus:

Originates in the sphenoid bone it's full size by late ten age years, The thickness of wall variable.It supplied by the sphenopalative artery.(Ameet singh et- al 2013).

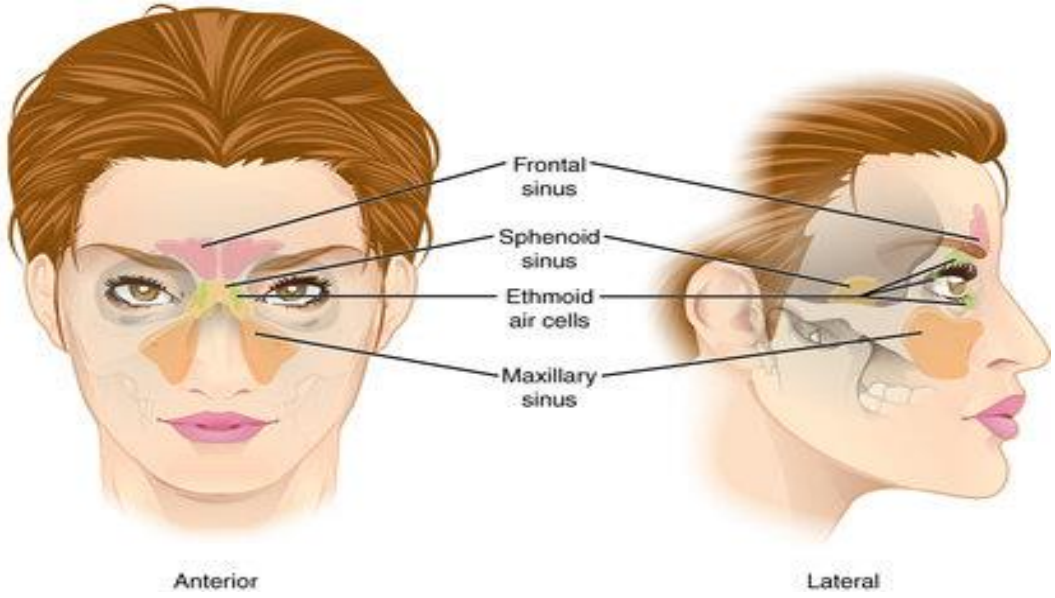

Figure 2.22 show anterior and lateral projection of paranasal sinuses

2.1.2 Physiology of para nasal sinuses:

Air conditioning, pressure dumping, heat in solution. Reduction of skull weight, flotation of skull in water increasing the olfactory area. Mechanical rigidity, vocal resonance and diminution of auditory fed back. Areas for production of mucus to moisten the nasal chambers and inspired air.

2.1.3 Pathology of Para nasal sinuses are

2.1.3.1 Sinusitis

It is inflammatory condition of the mucous membrane lining of the sinuses. It may progress to pus formation. May be acute and chronic and may be primary or secondary. Primary are appear as result of trauma or allergy. But usually infection from other focuses. There are 3 main factors lead to sinusitis development opening of sinus hole, may be blocked and may be an anomaly of anatomical structures. The retain of secret decrease the pressure of oxygen contribute the bacteria multiplication. (Slide share et – al 2010)

2.1.3.2 Cancer:

Cancer of Para nasal sinuses relatively un common. These can rang from benign and low grade malignant that can be removed via a minimally in naive endoscopic approach to tumors that are extremely aggressive and require removal of most or all of the entire cheek bone (maxilla) and occasionally the base of the Skull and eye as well. (board 2014)

2.1.3.3 Rhinitis:

Occurs when you breathe in something you are allergic to such as duts-dander or pollen(board 2014)

2.1.3.4 Polyps:

Are sac-like consisting of inflamed tissue to sinuses. Large polyps can block the sinuses(Slide share et – al 2010)

2.1.3.5 Mucosa thickening:

Is a common occurrence. It suggests mild sinusitis if sever sinusitis can cause headaches. Is a self-limiting and non-dangerous condition.

The voltage used in this study was fixed 120 kVp, the advantage of a high tube voltage and the corresponding high (average) photon energy is good transmission of x-rays, which results in relatively high detector dose and thus contributes to relatively low noise level in images. (Slide share et – al 2010)

2-2 previous studies:

Minseo Bang et al 2016 his study was aimed to compare the radiation dose of low-dose computed tomography (CT) to that of standard-dose CT, Second to determine the minimum optimal radiation dose for use in patients who need endoscopic sinus surgery, and third to assess the reliability of iterative model reconstruction, they found forty-eight patients were evaluated (17 women and 31 men). Patients' mean age was 43.1 6 13.2 years. The mean dose-length products were as follows: 14.62 6 1.02 for ULD CT, 29.23 6 2.01 for VLD CT, 57.10 6 3.96 for LD CT , and 239.35 6 16.63 for SD CT. The effective radiation doses were 0.033 6 0.002 mSv for ULD CT, 0.067 6 0.004 mSv for VLD CT, 0.131 6 0.008 mSv for LD CT, and 0.549 6 0.049 mSv for SD CT. The effective radiation dose was significantly lower for each LD CT protocol than for SD CT (approximately by 6% for ULD CT, 12% for VLD CT, and 22% for LD CT; P\.001, all)

Mohamed Yousef et al 2015 their study aimed to evaluate the role of computed tomography scan in the diagnosis of sinuses diseases. Subjects and Methods: This was a cross-sectional study design, conducted in different hospitals and clinical centers at Khartoum State. Totally 26 males and 24 females aged ranges from 10 to 70 years old with different symptoms were selected, axial and direct coronal cuts were done for all cases. Results: The study revealed that most patients were affected in the both sides, with a history of sinuses diseases in their families, maxillary sinuses are the most affected area, and most patients suffer from headache. Chronic and fungal sinusitis the sensitivity of the coronal view was (77%, 61%, and 61%) respectively compared to axial that was (22%, 36%, and 38%) respectively. In the nasal polyp and granulomatous diseases, the efficiency of the coronal view was (62% and 65%) respectively, while in axial was (37% and 34%) respectively. In benign and malignant tumor the efficiency of coronal was 57% and 32% respectively, while in the axial view was (42% and

21%) respectively. Conclusions: This study concluded that the two image planes are performed together and used as an essential technique of peripheral nerve stimulation.

Christian Güldner et al 2017 found the Preoperative imaging of the nose and paranasal sinus is standard in otorhinolaryngology. Previous studies on phantoms demonstrated the potential for dose reduction of cone beam computed tomography (CBCT) by varying the application parameters. Methodology. Based on previous studies, the standard protocol of paranasal sinus imaging by CBCT was altered.

One hundred and fifty examinations using the old protocol (01/2010–01/2011, high dosage) and 150 examinations using the new protocol (09/2012–09/2013, low dosage) were evaluated and compared for the visibility of 17 anatomical structures, the LundMackay Score, and technical parameters. Results. Alteration of the protocol resulted in a significant reduction in dosage (6.64 mGy versus 2.88 mGy). Both groups showed the same amount of pathology (Lund-Mackay Score: 4.95±3.79 versus 5.26±5.77; $p = 0.558$).

There was a significant better visibility of the anatomical structures (all visible = 1, nothing visible = 4) (results: 1.25 versus 1.17; $p = 0.001$) inthelow-dosagegroup. Conclusion. Despite a significant reduction in the applied dosage, reliable visualization of the bony anatomy of the anterior skull base is possible by CBCT. This demonstrates the need for the discussion of the required clinical imaging quality.

Lars-Arne Schaafs et al 2016 were evaluate the feasibility and image quality of low-dose CT of the paranasal sinuses using iterative reconstruction with adaptive-iterative dose reduction in three dimensions (AIDR 3D) in comparison with conventional image protocols of older scanner generations . Sinus CT scans of 136 patients were assessed retrospectively. Patients underwent CT either with low-dose settings (Protocol A: 80 kV, 30 mA s; Protocol B: 120 kV, 15 mA s or

C: 80 kV, 90 mA s) reconstructed using AIDR 3D (Protocols A and B) or filtered back projection (FBP) (Protocol C) or with standard dose (Protocol D: 120 kV, 80 mA s) and FBP. Mean ED could be lowered by 82% when using Protocol A. The best image quality was found using Protocol B (mean score52.1 ± 0.51). Conspicuity of relevant anatomic landmarks was best with Protocol A (mean score511.97 ± 1.88). Protocol B provided the highest conspicuity of osseous structures (mean score58.27 ± 1.58). Image noise was highest in images obtained using Protocol A. AIDR 3D allows a significant dose reduction while maintaining a good diagnostic image quality and conspicuity of relevant anatomic structures. Dentomaxillo facial Radiology (2016) .

J.M. Hoxworth et al 2013 found that the CT performed with Veo model-based iterative reconstruction has shown the potential for radiation dose reduction. This study sought to determine whether Veo could reduce noise and improve the image quality of low-dose sinus CT. RESULTS: Eight women and 12 men (mean age, 63.3 years) participated. Volume CT dose indices were 2.9 mGy (low dose) and 31.6 mGy (standard dose), and mean dose-length products were 37.4 mGy-cm (low dose) and 406.1 mGy-cm (standard dose). Of all the imaging series, low-dose Veo demonstrated the least noise (*P* _ .001). Compared with filtered back-projection low-dose CT using soft-tissue and bone algorithms, Veo had the best soft-tissue image quality but the poorest bone image quality (*P*_ .001). CONCLUSIONS: Veo significantly reduces noise in low-dose sinus CT. Although this reduction improves soft-tissue evaluation, thin bone becomes less distinct .

CHAPTER THREE

MATERIALS AND METHODS

3.1 Materials

3.1.5. Machine used:

The CT images were conducted using multi-detector CT scanner .The scan parameters (thin section 5mm or less ,120 KV ,200 MA,1.5 pitch)Features of CT scanner : Largest couch capacity is 180 Kg ,CT machine in Ibn ELHaytham Diagnostic Center .

3.1.1 Study design: This is descriptive and analytic study.

3.1.2 Area of study

This study was performed at radiology department in Ibn ELhaithm Diagnostic Center.

3.1.3 Duration of study

From February to August 2018.

3.1.4. Inclusion criteria

All age groups, all patients with clinical suspicion of CT PNS exam.

3.1.5. Exclusion criteria: All pregnant women

3.2. Methods

3.2.1. Technique

The patient should wear comfortable , loose-fitting clothing to your exam ,you may be given a gown to wear during the procedure, metal object including jewelry ,eyeglasses ,hairpins should be removed prior the exam .if the contrast agent is request the patient must be fasted 4-6 h before the exam .asked patient don’t move during the scan .patient should be lying supine with the head in axial head holder ,scan should be parallel to the OML .the gantry was tilted (0-10) degree, we use (3-5) mm slice thickness should be taken forward the entire face .we use 2000-2500 HU window width ,200-350 HU window level ,this provides details of bone and soft tissues on a single set of film . Straps and pillows may be used to maintain the correct position and to hold still during the exam when the

examination is completed ,you will be asked to wait until the technologist verifies that the images are of high enough quality for accurate interpretation. we use post processing reformat for further views in different plane (coronal and Sagittal) from the axial projection .

3.2.2. Data collection

Using data collection sheet.

3.2.3. Data analysis

Data were first summarized into master data sheet, then analyzed by SPSS program and then used Microsoft excel (variables using descriptive tables frequency, percentage distribution tables, cross tabulation) for data presentation.

3.2.4. Data presentation:

Tables and Bar chart

3.2.5. Ethical considerations:

Verbal concept was taken from the patient to be included in this study.

CHAPTER FOUR

THE RESULTS

Chapter Four

Results

4.1 The Results

Table 4.1 Shows the mean of age, Kvp, mA ,exposure, computed tomography dose index volum (CTDIvol),dose length product (DLP) and effective dose(ED) in this study.

	Minimum	Maximum	Mean	Std. Deviation
Age	18	85	38.38	17.156
Kvp	120	120	120.00	.000
mA	75	157	100.54	24.938
Exposure	27	13386	2388.07	3205.407
CTDIvol	32.4	129.9	52.704	25.0821
DLP	216.7	1541.0	577.084	267.4298
ED	3.3	23.1	8.656	4.0114

Table 4.2 Shows the frequency for age group.

Age Group	Frequency	Percent
18-30	22	44.0
31-40	9	18.0
41-50	8	16.0
51-60	5	10.0
61-70	3	6.0
71-85	3	6.0
Total	50	100.0

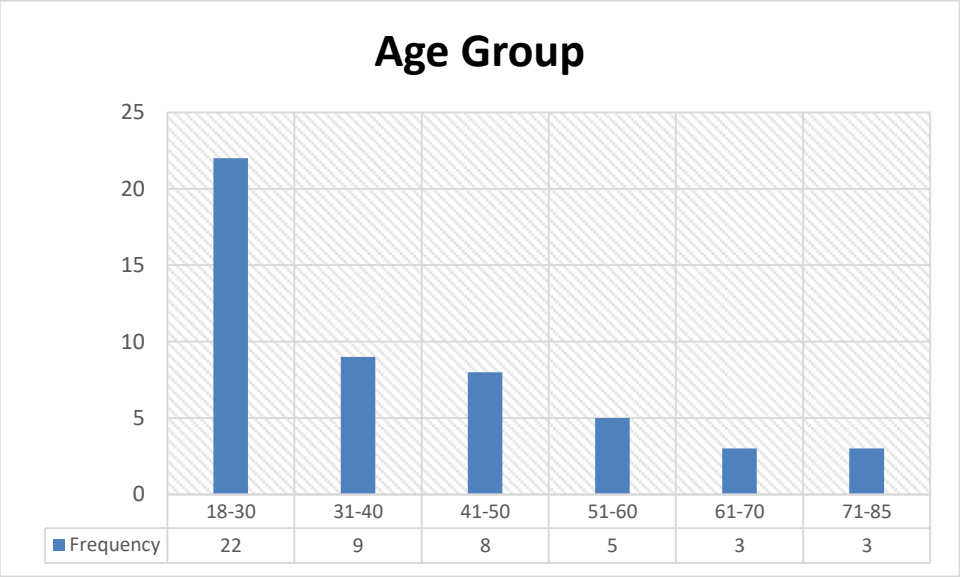

Figure 4.1 shows the frequency for age group

Table 4.3 Shows the correlation between effective dose (ED) and age group

ED mSv * Age Group Crosstabulation

ED mSv	Age Group						Total
	18-30	31-40	41-50	51-60	61-70	71-85	
3-7	8	4	5	3	0	1	21
7.1-11	8	3	3	2	3	0	19
11.1-15	3	1	0	0	0	0	4
15.18	3	1	0	0	0	2	6
Total	22	9	8	5	3	3	50

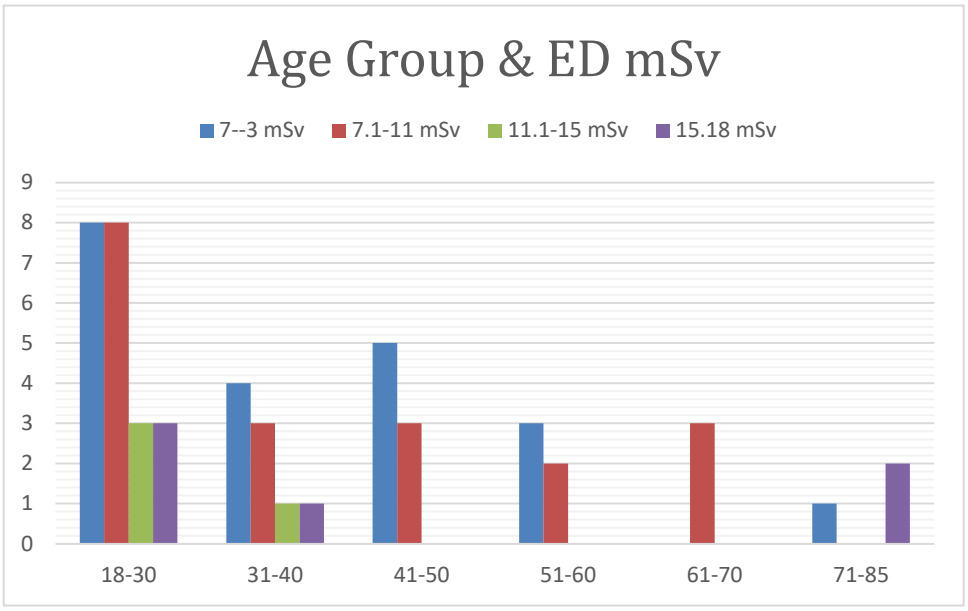

Figure 4.2 shows the correlation between effective dose(ED) &age group

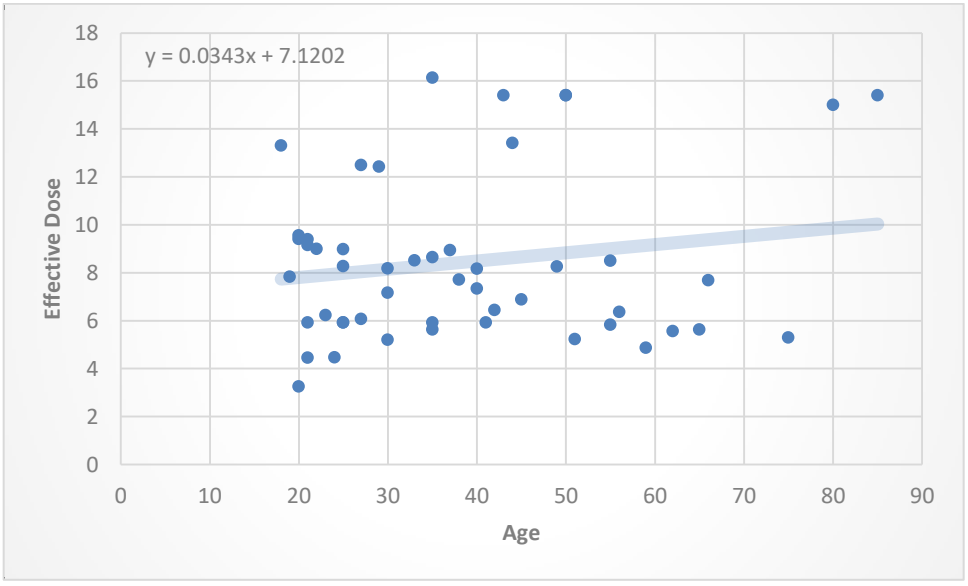

Figure 4.3 shows the correlation between effective dose(ED) &age

CHAPTER FIVE

Discussion, Conclusion and Recommendations

5.1 Discussion:

Table 4.1 show statistical parameters for all patients were the data presented as mean, STD, Minimum and Maximum were the age was38.38±17.16 , KVP120.00±000,mA100.54±24.94,exposure2388.07±3205.41,CTDIvol52.7±25.1 , DLP577.1±267.43 and ED8.66±4.0114 .

Table 4.2 Show frequency distribution for age group were the group 18-30 years was 22 with percentage 44.0 ,then group 31-40 years was 9 with percentage 18.0 , group 41-50 years was 8 with percentage 16.0 , group 51-60 years was 5 with percentage 10.0 and lowest groups 61-70 ,71-85 years were 3 with percentage 6.0 .

Table 4.3 show cross-tabulation for ED mSv with the age group ,were the dose group 3-7 mSv with 21 patients , the dose group 7.1-11 mSv with 19 patients , the dose group 11,1-15 mSv with 4 patients and the dose group 15-18 mSv with 6 patients .

Figure 4.1 shows the frequency for age group were the group 18-30 years was 22 with percentage 44.0 ,then group 31-40 years was 9 with percentage 18.0 , group 41-50 years was 8 with percentage 16.0 , group 51-60 years was 5 with percentage 10.0 and lowest groups 61-70 ,71-85 years were 3 with percentage 6.0 .

Figure 4.2 shows the correlation between effective dose(ED) &age group were the dose group 3-7 mSv with 21 patients , the dose group 7.1-11 mSv with 19 patients , the dose group 11,1-15 mSv with 4 patients and the dose group 15-18 mSv with 6 patients .

Figure 4.3 shows the correlation between effective dose(ED) &age (y=0.0343x+7.1202) .

5.2 Conclusion:

A reduction of tube voltage alone would increase image noise considerably and image quality would probably deteriorate to a level that is unacceptable to the radiologist. In general, reduction of tube voltage should necessarily be accompanied by some increase in radiographic exposure (mAs). Such an increase is acceptable as long as the combination of reduced tube voltage and increased radiographic exposure yields an effective dose that is equal to or lower than the initial effective dose. Ideally, radiographic exposure should be increased enough to maintain the initial image quality, or initial contrast-to-noise ratio, whilst achieving a reduction in patient effective dose.

5.3 Recommendations:

- MSCT imaging protocols in CT imaging should be standardized across. Departments with the aim of reducing dose variation across patients and facilities.
- Physicians need to follow guidelines for reducing dosages, such as national dose references level for radiation dose, and they are recommended to participate in the radiation dose registry to obtain feedback on radiation dose levels compared to other department.
- Utilization of MSCT angiography must be defined as whether it leads to the greatest benefit and whether the radiation risk may be greater than the benefit expected from the CT examinations.
- Urgent training programs highly recommended to improve patient protection in CT examinations.
- Further, study in radiation dose during CT PNS with large sample size is recommended .

References:

Ana Teresa .2011. Casimiro Nunes, Faculdade de Ciencias e Technologia Universidade de Coimbra, M.Sc. Thesis,.

Anne Paterson, Donad P. Frush, and Lane Donnely, Feb 2001. "Helical CT of the body: Are setting adjusted for pediatric patient?" AJR Vol.176. pp. 297-301.

Brenner DJ, Hall EJ. 2007 .Computed tomography: an increasing source of radiation exposure. N Engl J Med; 357: 2277-2284.

Cattin, P. 2010. Principles of Medical Imaging. [Presentation] Basel: University of Basel.

Elaine N. 2010. Marieb Human Anatomy & Physiology.

Kalender WA, Wolf H, Suess C, Gies M, Greess H, Bautz WA. 1999 .Dose reduction in CT by on-line tube current control: principles and validation on phantoms and cadavers. Eur Radiol 1999; 9:323-328.

Shrimpton PC, Edyvean S. 1998 .CT scanner dosimetry. Br J Radiol 1998; 71:1-3.

Martin CJ: 2007 Effective dose: how should it be applied to medical exposures? Br J Radiol. 2007; 80:639–47.

Kalender, W.A. 2005 .Computed tomography: fundamentals, system technology, image quality, applications. Chichester : Wiley,.

McCollough CM, Schueler BA. 2000 .Calculation of effective dose. Med Phys 2000; 27:838-844.

Rehani M, Berry M. 2000. Radiation doses in computed tomography (Editorial). Br. Med. J. 320, 593-594. 2000.

Lewis M, Keat N, Edyvean S. March 26, 2008 16 Slice CT scanner comparison report version 14. Report 06012, Feb-06. March 26, 2008.

Appendix

Data collection sheet

Exam	*Age*	*kvp*	*mA*	*Slice thikness*	*Exposure time/s*	*CTDI|vol(mGy)*	*DLP(mGy-cm)*